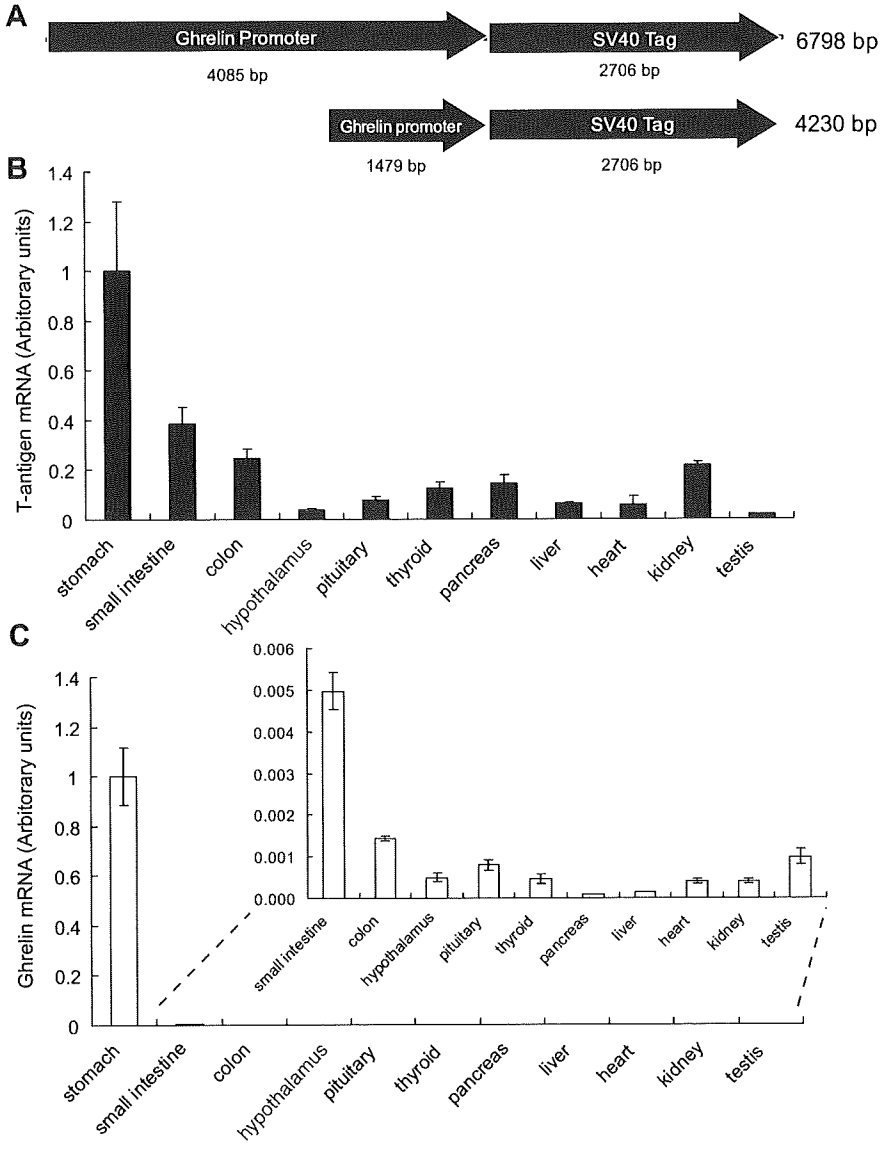

Fig. 1. Constructs of ghrelin promoter-SV40 T-antigen transgenic (GP-Tag Tg) mice and the expression levels of SV40 T-antigen mRNA in various tissues. *A*: 2 types of fusion genes comprising 5′-flanking region of human ghrelin gene (4,085 or 1,479 bp) and SV40 Tag were designed. *B*: the expression levels of SV40 T-antigen mRNA in various tissues of GP-Tag Tg mice at 6 wk of age (n = 8). SV40 T-antigen mRNA was most abundant in the stomachs of GP-Tag Tg mice. *C*: the expression levels of ghrelin mRNA in various tissues of nontransgenic littermates at 6 wk of age (n = 4).

Southern blot analysis of tail DNAs. Transgenic mice were used as heterozygotes. Animals were maintained on standard rodent food (CE-2, 352 kcal/100 g; Japan CLEA, Tokyo, Japan) on a 12:12-h light-dark cycle unless otherwise indicated. All experimental procedures were approved by the Kyoto University Graduate School of Medicine Committee on Animal Research.

RT-PCR and real-time quantitative RT-PCR. Total RNA was extracted using a Sepasol RNA kit (Nacalai Tesque, Kyoto, Japan). Reverse transcription was performed with a high-capacity cDNA reverse transcription kit (Applied Biosystems, Foster City, CA). RT-PCR was carried out with a GeneAmp 9700 using primers in Table 1 with AmpliTaq Gold PCR master mix (Applied Biosystems). Real-time quantitative PCR was performed using an ABI PRISM 7500 Sequence Detection System (Applied Biosystems) with primers and TaqMan probes or with Power SybrGreen (presented in Table 1). The mRNA expression in each gene was normalized to levels of 18S ribosomal RNA.

Immunohistochemistry. Formalin-fixed, paraffin-embedded tissue sections were immunostained using the avidin-biotin peroxidase complex method (Vectastain "ABC" Elite kit; Vector Laboratories, Burlingame, CA), as described previously (18). Sections were incubated with anti-COOH-terminal ghrelin (AA 13-28) (1:2,000 at final dilution), anti-NH_2-terminal ghrelin (14) that recognizes the n-octanoylated portion of ghrelin (AA 1-11) (1:5,000), anti-glucagon (1:500; DAKO, Glostrup, Denmark), anti-somatostatin (1:500; DAKO), anti-gastrin (1:500; DAKO), and anti-GH (1:500; DAKO). The cell number of ghrelin-immunopositive cells was analyzed by WinRoof visual analysis software (Mitani, Fukui, Japan).

Measurements of plasma and tissue ghrelin concentrations. Collection of plasma samples was performed as reported previously (18). Plasma ghrelin and desacyl ghrelin concentrations were determined using two separate ELISA kits, an active ghrelin ELISA kit that recognizes n-octanoylated ghrelin and a desacyl ghrelin ELISA kit (both from Mitsubishi Kagaku Iatron, Tokyo, Japan) (1). Tissue ghrelin concentration was determined by radioimmunoassay (RIA) using anti-ghrelin (AA 13-28) antiserum (C-RIA) and anti-ghrelin (AA 1-11) antiserum (N-RIA), as described previously (18).

Western blot. Stomachs were boiled for 5 min in the 10-fold vol/wt of water. Acetic acid was added to each solution so that the final concentration was adjusted to 1 M, and the tissues were homogenized.

Table 1. *PCR primers and TaqMan probes*

Gene	Primer Sequence
Ghrelin	
Sense	5′-GCATGCTCTGGATGGACATG-3′
Antisense	5′-TGGTGGCTTCTTGGATTCCT-3′
TaqMan probe	5′-AGCCCAGAGCACCAGAAAGCCCA-3′
NPY	
Sense	5′-TCCGCTCTGCGACACTACAT-3′
Antisense	5′-GGAAGGGTCTTCAAGCCTTGT-3′
TaqMan probe	5′-CAAGGGCTGGATCTCTTGCCATATCTCTG-3′
AgRP	
Sense	5′-GCTCCACTGAAGGGCATCA-3′
Antisense	5′-TAGCACCTCCGCCAAAGCT-3′
TaqMan probe	5′-TTCCCAGGTCTAAGTCTGAATGGCCTCA-3′
GHRH	
Sense	5′-AGGATGCAGCGACACGTAGA-3′
Antisense	5′-TCTCCCCTTGCTTGTTCATGA-3′
TaqMan probe	5′-CCACCAACTACAGGAAACTCCTGAGCCA-3′
Somatostatin	
Sense	5′-AGCTGAGCAGGACGAGATGAG-3′
Antisense	5′-ACAGGATGTGAATGTCTTCCAGTT-3′
TaqMan probe	5′-CGAACCCAGCAATGGCACCCC-3′
GHS-R	
Sense	5′-CACCAACCTCTACCTATCCAGCAT-3′
Antisense	5′-CTGACAAACTGGAAGAGTTTGCA-3′
TaqMan probe	5′-TCCGATCTGCTCATCTTCCTGTGCATG-3′
GH	
Sense	5′-AAGAGTTCGAGCGTGCCTACA-3′
Antisense	5′-GAAGCAATTCCATGTCGGTTC-3′
TaqMan probe	5′-CCATTCAGAATGCCCAGGCTGCTTTC-3′
GHRH-R	
Sense	5′-GCCCTTGGAACTGTTAACCA-3′
Antisense	5′-GCAACCAGGATGGCAATAGC-3′
TaqMan probe	5′-AGCATCTCCATTGTAGCCCTCTGCGTG-3′
SV40 Tag	
Sense	5′-AAACACTGCAGGCCAGATTT-3′
Antisense with power SYBR Green	5′-AAATGAGCCTTGGGACTGTG-3′
PC1/3	
Sense	5′-AGTGGAAAAGATGGTGAATG-3′
Antisense	5′-CTCCTCATTTAGGATGTCCA-3′

NPY, neuropeptide Y; AgRP, agouti-related protein; GHRH, growth hormone (GH)-releasing hormone; GHS-R, GH secretagogue receptor; GHRH-R, GHRH receptor; PC1/3, prohormone convertase 1/3.

The supernatant was loaded onto a Sep-Pak C18 cartridge (Waters, Milford, MA) preequilibrated with 0.9% NaCl after centrifugation. The cartridge was washed with 2.5 ml of 5% CH_3CN-0.1% trifluoroacetic acid and eluted with 2.5 ml 60% CH_3CN-0.1% trifluoroacetic acid. The eluate was evaporated, lyophilized, and dissolved in Novex Tricine SDS Sample Buffer (Invitrogen, Carlsbad, CA). After being heated at 85°C for 2 min, 20 mg of samples of initial weight were subjected to tricine-SDS PAGE and electroblotted to polyvinylidene fluoride membranes (Invitrogen). Transferred membranes were blocked with Immunoblock (Dainippon Seiyaku, Osaka, Japan) and then incubated with anti-COOH-terminal ghrelin antibody (1:5,000). After being washed with PBS-0.1% Tween-20, membranes were reacted with secondary antibodies and developed with ECL plus (GE Healthcare, Buckinghamshire, UK) as instructed by the manufacturer. The signal on the blot was detected with Lumino-Image Analyzer LAS-3000 mini system (Fuji Photo Film, Tokyo, Japan).

Measurement of food intake. Mice were housed individually with continuous access to chow and water. Food intakes were measured by subtracting the remaining weight of the chow from that originally presented. As for measuring the food intake by ghrelin, ad libitum-fed mice were injected with ghrelin (120 or 360 μg/kg) or saline subcutaneously. Food intakes were measured for 2 h after injection.

Measurements of lean body mass, fat mass, and bone mass. Mice were anesthetized with pentobarbital sodium. Lean body mass, fat mass, and bone mass of mice were measured by an animal computed tomography system (Latheta LTC-100; Aloka, Tokyo, Japan).

Measurements of hormones and blood glucose levels. Serum GH levels were determined by a rat GH EIA kit (SPI Bio, Massy Cedex, France). Serum insulin-like growth factor I (IGF-I) levels were measured using a mouse IGF-I immunoassay kit (R & D Systems, Minneapolis, MN). Blood glucose levels were determined by glucose oxidase method using Glutest Sensor Neo (Sanwa Kagaku, Kyoto, Japan). Measurement of serum insulin concentrations was performed by ELISA using an ultrasensitive rat insulin kit (Morinaga, Yokohama, Japan).

GH-provocative test. GH-provocative test was carried out as described previously (16). Serum samples were collected at 15 min after subcutaneous injection of 180 μg/kg of GH-releasing hormone (GHRH) or 120 μg/kg of ghrelin. We choose these doses according to the results of our previous study (16).

Glucose and insulin tolerance tests. For the glucose tolerance test, after overnight fast, the mice were injected with 1.5 g/kg glucose intraperitoneally. For the insulin tolerance test, after a 4-h fast, mice were injected with 1.0 mU/g human regular insulin (Novolin R; Novo Nordisk, Bagsvaerd, Denmark) intraperitoneally. Blood was sampled from the tail vein before and 30, 60, 90, and 120 min after the injection.

Insulin release. After overnight fast, the mice were injected with 3.0 g/kg glucose intraperitoneally. Blood was sampled from the retroorbital vein at 2 and 30 min after the injection using a glass tube.

Statistical analysis. All values were expressed as means ± SE. The statistical significance of the differences in mean values was assessed by repeated-measures ANOVA or Student's *t*-test. The statistical difference in the changes of plasma ghrelin levels by feeding were assessed by paired *t*-test. Pearson's correlation coefficient analysis and simple regression were used to assess the relations between plasma ghrelin level and body weight. Difference of correlation coefficients of the regression lines obtained from GP-Tag Tg mice and nontransgenic littermates was determined by testing the *t* value.

RESULTS

Generation of GP-Tag Tg mice. By injecting transgenes into 846 eggs, we obtained 11 lines of GP (4.85) Tag Tg mouse. We succeeded in breeding three of these lines (1-5, 3-1, and 4-3). Among these three lines, mice of the 3-1 line developed gastric tumor and showed elevated plasma ghrelin levels, as described below. Mice of the 1-5 line showed very aggressive tumor development and died at ~13 wk of age because of thyroid, pancreatic, and gastric tumors. Mice of the 4-3 line showed very slow tumor development. The proliferation of ghrelin cells was

Fig. 2. Pathological findings and tissue ghrelin concentrations of stomachs in GP-Tag Tg mice. *A–C*: macro findings of stomachs in GP-Tag Tg mice (*A*: arrow, dotted area; *B*: Tg) and nontransgenic littermates (non; *B*) at 12 wk of age. Stomach walls of GP-Tag Tg mice were hypertrophic. *C*: immunohistochemical analysis of ghrelin peptide expression in tissue sections of stomachs of GP-Tag Tg mice (Tg) and nontransgenic littermates (non) using anti-COOH-terminal and anti-NH_2-terminal ghrelin antibodies. *D*: the cell number of ghrelin-immunopositive cells in Tg and non littermates. *E*: the mRNA levels of ghrelin in 12-wk-old male Tg mice and non littermates; $n = 5$, $^{**}P < 0.01$ compared with nontransgenic littermates. *F* and *G*: tissue concentration per milligram (*F*) and per stomach (*G*) of ghrelin peptide in 12-wk-old male Tg mice (black bars) and non littermates (open bars); $n = 6$, $^{**}P < 0.01$ compared with non littermates. C-RIA, total ghrelin (ghrelin and desacyl ghrelin); N-RIA, ghrelin. *H*: Western blot analysis of stomach samples of Tg and non littermates using anti COOH-terminal ghrelin antibody. *I*: RT-PCR analysis of prohormone convertase 1/3 (PC1/3) mRNA expression in the stomach of Tg.

modest even at 50 wk of age in the 4-3 line. Accordingly, we analyzed mainly GP-Tag Tg mice of the 3-1 line.

We could not get a transgene-positive mouse of GP (1479) Tag Tg mouse by injecting transgenes into 631 eggs.

The expression levels of SV40-Tag mRNA among various tissues. We first examined the expression levels of SV40-Tag mRNA in various tissues of GP-Tag Tg mice, including stomach, small intestine, colon, hypothalamus, pituitary, thyroid,

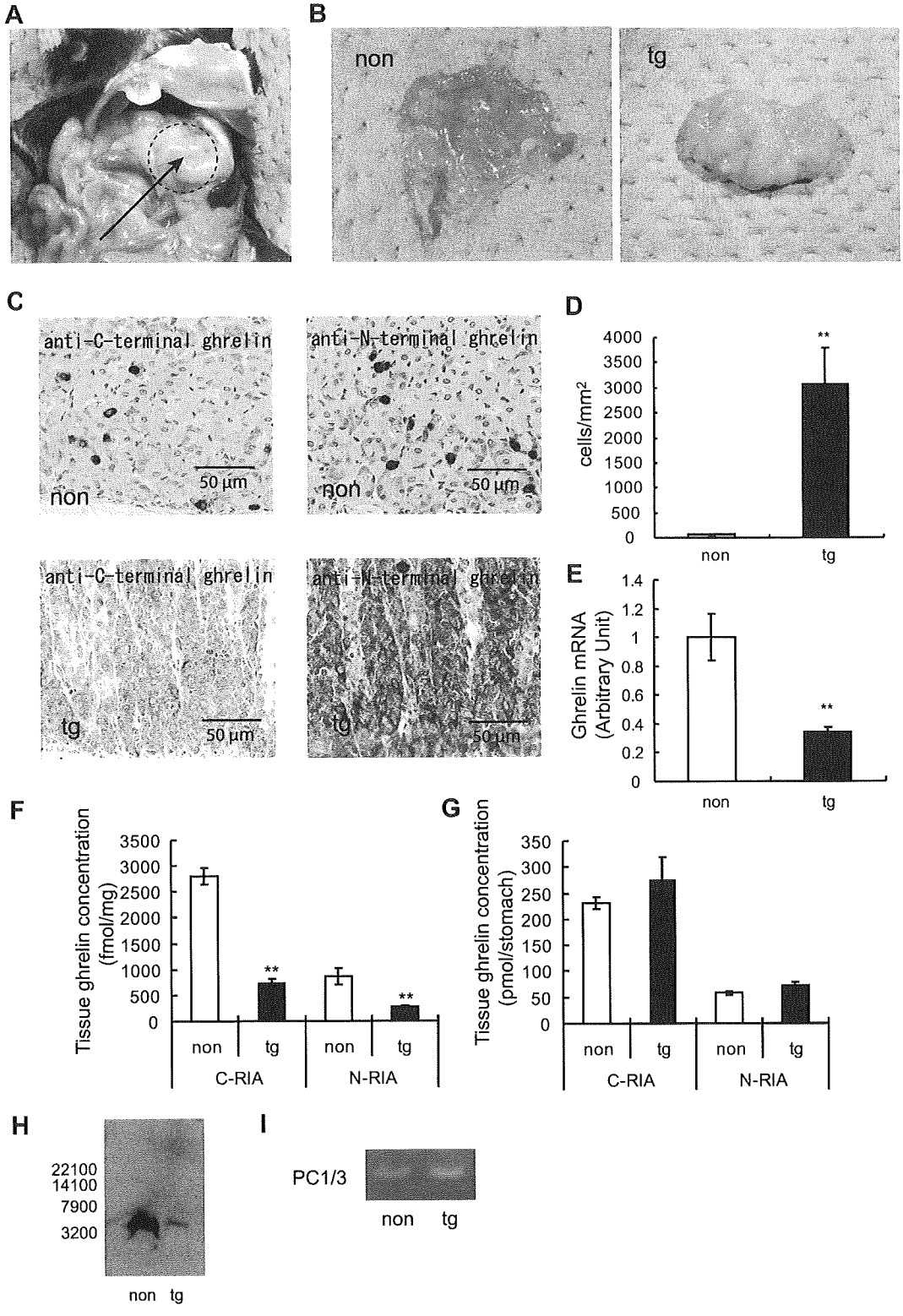

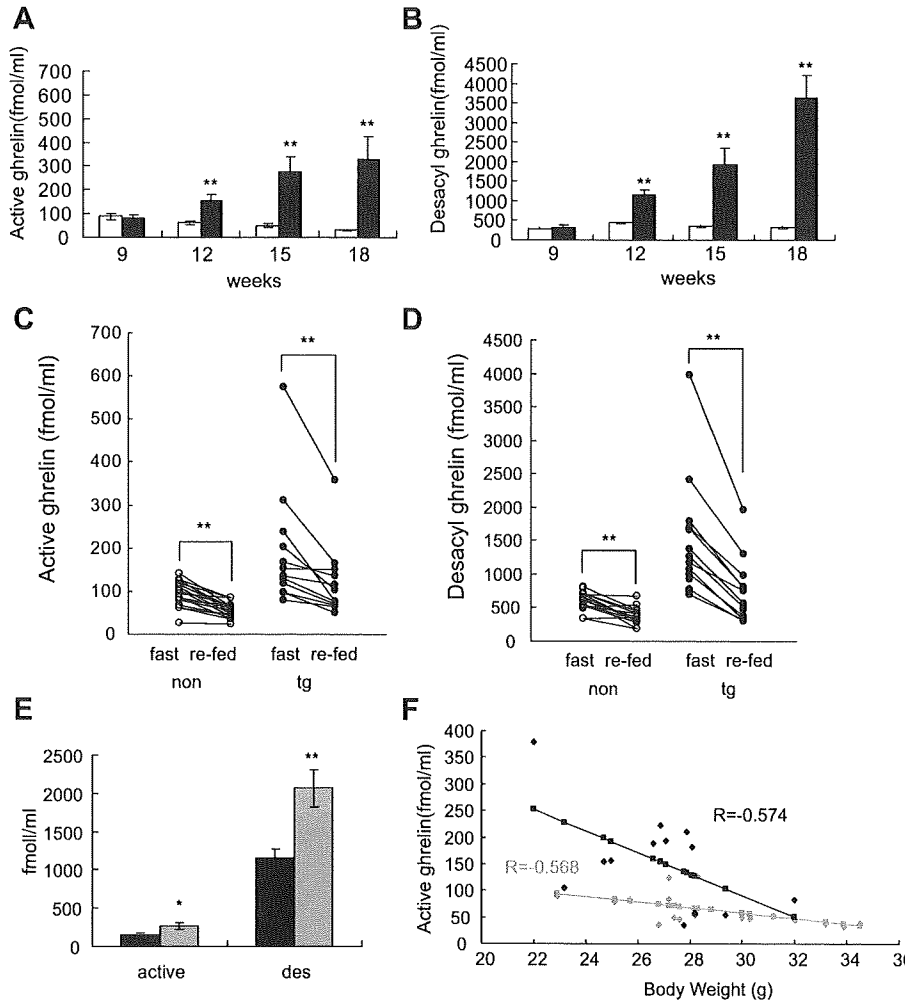

Fig. 3. Plasma ghrelin and desacyl ghrelin levels in GP-Tag Tg mice. *A* and *B*: plasma ghrelin (*A*) and desacyl ghrelin (*B*) levels in male GP-Tag Tg mice (black bars) and nontransgenic littermates (open bars); $n = 3$–17. $^{**}P < 0.01$ compared with non littermates. *C* and *D*: plasma ghrelin (*C*) and desacyl ghrelin (*D*) levels after overnight fasting (fast) and after refeeding (refed) in 15-wk-old male Tg and non mice. $^{**}P < 0.01$; $n = 12$–18. *E*: plasma ghrelin (active) and desacyl ghrelin (des) levels in 12-wk-old male (black bars) and female (gray bars) GP-Tag Tg mice; $n = 7$–13, $^{*}P < 0.05$, $^{**}P < 0.01$ compared with male GP-Tag Tg mice. *F*: plasma ghrelin levels were correlated with body weights in 12-wk-old male GP-Tag Tg mice (black bars; $r = -0.574$, $P < 0.01$) and in nontransgenic littermates (gray bars; $r = -0.568$, $P < 0.05$). The regression coefficient of the regression line of GP-Tag Tg mice was bigger than that of nontransgenic littermates ($t = 2.08$, $P < 0.05$).

pancreas, liver, heart, kidney, and testis (Fig. 1*B*). The highest expression levels were observed in stomach, and the second-highest levels were observed in small intestine. The expression pattern of SV40-Tag mRNA was almost similar to that of ghrelin (Fig. 1*C*).

Pathological feature and tissue ghrelin concentration of stomach of GP-Tag Tg mice. Stomach walls of GP-Tag Tg mice became hypertrophic with age (Fig. 2, *A* and *B*). Immunohistochemical analysis by both anti-COOH-terminal and anti-NH_2-terminal ghrelin antibodies revealed hyperplasia of ghrelin-immunopositive cells (Fig. 2, *C* and *D*), although the staining in GP-Tag Tg mice was paler than that in nontransgenic littermates (Fig. 2*C*). These hyperproliferating cells were not immunostained with anti-glucagon, somatostatin, or gastrin antibodies (data not shown).

The mRNA levels of ghrelin in the stomachs of 12-wk-old male GP-Tag Tg mice were significantly lower than those of nontransgenic littermates ($P < 0.01$, $n = 6$; Fig. 2*E*). Consistent with this observation, tissue concentrations of ghrelin (N-RIA; fmol/mg tissue) and total ghrelin (desacyl ghrelin plus ghrelin) (C-RIA) of 12-wk-old male GP-Tag Tg mice were significantly lower than those of nontransgenic littermates ($P < 0.01$, $n = 6$; Fig. 2*F*). However, since the weights of the stomach of GP-Tag Tg mice were significantly higher than controls (non-Tg vs. Tg, 83.4 vs. 362.0 mg, $P < 0.01$) due to the hypertrophy of the stomach wall, the tissue ghrelin concentration per whole stomach tended to be higher in GP-Tag Tg mice [not significant (NS), $n = 6$; Fig. 2*G*]. The size of ghrelin content of GP-Tag Tg mice was similar to that of nontransgenic littermates when analyzed by tricine-SDS PAGE and Western blot analysis (Fig. 2*H*), indicating that processing of preproghrelin to ghrelin occurred in hyperproliferaing ghrelin cells in GP-Tag Tg mice. The mRNA of prohormone convertase 1/3, which processes preproghrelin to ghrelin, was detected in the stomachs of GP-Tag Tg mice (Fig. 2*I*).

Plasma ghrelin levels of GP-Tag Tg mice. Plasma ghrelin and desacyl ghrelin levels of GP-Tag Tg mice were almost equal to those of nontransgenic littermates at 9 wk of age and then increased with age ($n = 3$–17; Fig. 3, *A* and *B*), with some variations in the levels among animals.

We next examined whether physiological regulation of ghrelin secretion is preserved in GP-Tag Tg mice. Plasma ghrelin and desacyl ghrelin levels of GP-Tag Tg mice were increased by fasting and decreased by refeeding $P < 0.01$, ($n = 7$–13; Fig. 3, *C* and *D*). Plasma ghrelin and desacyl ghrelin levels of female GP-Tag Tg mice were significantly higher than those of

male GP-Tag Tg mice at 12 wk of age (Fig. 3*E*). Plasma ghrelin levels of 12-wk-old male GP-Tag Tg mice correlated to body weight ($r = 0.574$, $P < 0.05$, $n = 13$; Fig. 3*F*). The regression coefficient of the regression line of GP-Tag Tg mice was bigger than that of nontransgenic littermates ($t = 2.08$, $P < 0.05$) These results indicate that regulation of plasma ghrelin and desacyl ghrelin levels of GP-Tag Tg mice were preserved, at least with regard to feeding status, body weight, and sex difference.

Body weights, body composition, and food intake of GP-Tag Tg mice. There was no difference in body weights between male GP-Tag Tg mice and controls until 12 wk of age ($n = 22$–34; Fig. 4*A*). After 13 wk of age, the body weights of the male GP-Tag Tg mice were significantly lower than those of nontransgenic littermates concomitantly with the decrease in the food intakes of male GP-Tag Tg mice after 11 wk of age (Fig. 4, *A* and *B*). When the body compositions were examined by computed tomography scan, fat masses were significantly reduced in 15-wk-old male GP-Tag Tg mice ($P < 0.05$, $n = 7$–9; Fig. 4*C*), whereas lean body masses and body lengths were not changed (NS, $n = 7$–9; Fig. 4, *D* and *E*). We also examined hypothalamic mRNA levels of neuropeptide Y (NPY), agouti-related protein (AgRP), and GHS-R in 12-wk-old male GP-Tag Tg mice. No significant changes were observed in these mRNA levels (NS, $n = 7$; Fig. 4*F*). When 15-wk-old male GP-Tag Tg mice were injected with ghrelin, the food intake was stimulated to the same extent as in controls (NS, $n = 10$–18; Fig. 4*G*). Plasma leptin levels of 15-wk-old male GP-Tag Tg mice were significantly lower than controls ($P < 0.05$, $n = 6$; Fig. 4*H*).

GH-IGF-I axis in GP-Tag Tg mice. Serum IGF-I levels of 12- and 15-wk-old male GP-Tag Tg mice were significantly higher than those of nontransgenic littermates ($P < 0.05$, $n = 7$–8, and $P < 0.05$, $n = 6$–7, respectively; Fig. 5*A*). Although basal serum GH levels of 15-wk-old male GP-Tag Tg mice were not significantly different from controls, serum GH levels after GHRH injection tended to be high ($P = 0.077$, $n = 8$–13), which was not observed after ghrelin injection (Fig. 5*B*). We then investigated the effects of chronic ghrelin elevation on hypothalamic and pituitary mRNA levels of components involved in GH regulation. There were no differences in hypothalamic mRNA levels of GHRH and somatostatin or in pituitary mRNA levels of GH and GHRH receptor (GHRH-R) between 15-wk-old male GP-Tag Tg mice and their littermates

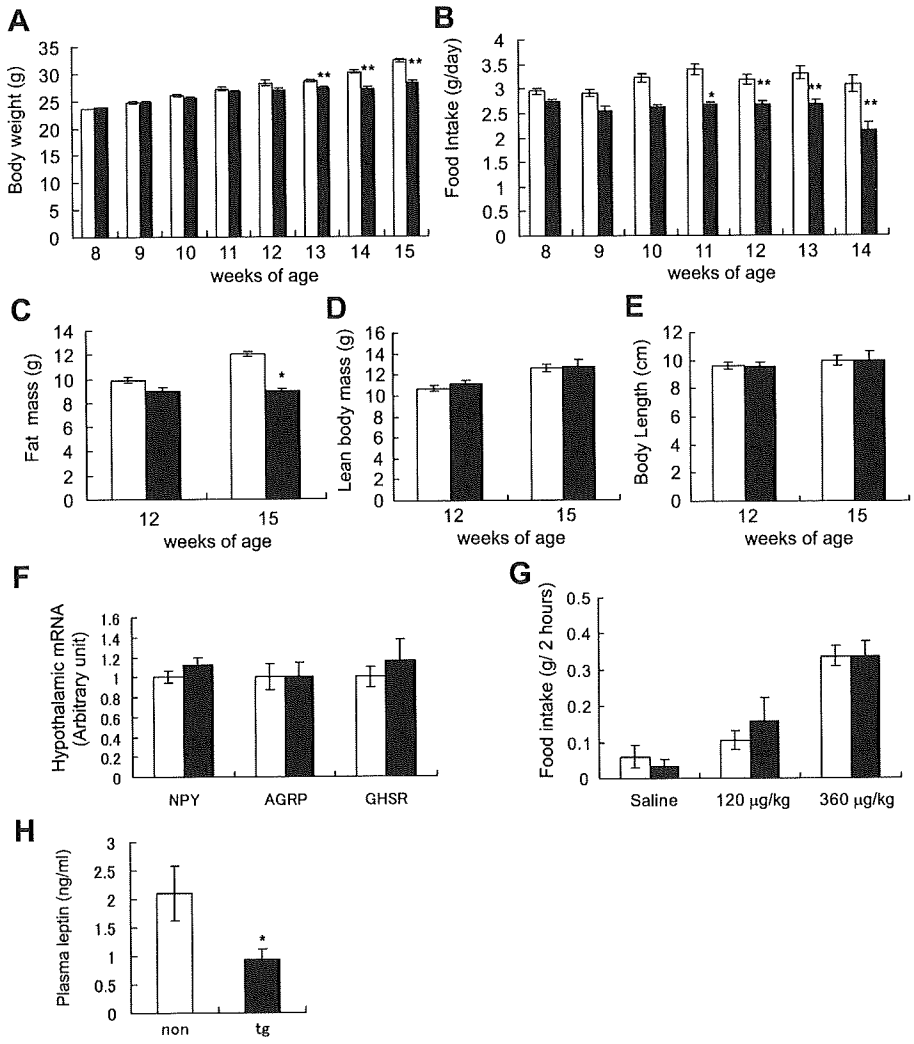

Fig. 4. Body weights, body compositions, and food intakes of GP-Tag Tg mice. *A*: body weights of male GP-Tag Tg mice (black bars) and nontransgenic littermates (open bars); $n = 22$–34. *B*: daily food intakes of male GP-Tag Tg mice (black bars) and nontransgenic littermates (open bars); $n = 19$–26. *C* and *D*: fat mass (*C*) and lean body mass (*D*) determined by animal computed tomography scan of 15-wk-old male GP-Tag Tg mice (black bars) and nontransgenic littermates (open bars). *E*: body length of 15-wk-old male GP-Tag Tg mice (black bars) and nontransgenic littermates (open bars); $n = 7$–9. *F*: hypothalamic mRNA levels of neuropeptide Y (NPY), agouti-related protein (AgRP), and growth hormone secretagogue receptor (GHS-R) in 12-wk-old male GP-Tag Tg mice (black bars) and nontransgenic littermates (open bars); $n = 7$. *G*: food intake for 2 h after injection of ghrelin (120 or 360 μg/kg or saline; $n = 10$–18). *H*: plasma leptin levels in 15-wk-old male Tg mice (black bars) and non littermates (open bars); $n = 6$–7. $^*P < 0.05$, $^{**}P < 0.01$ compared with nontransgenic littermates.

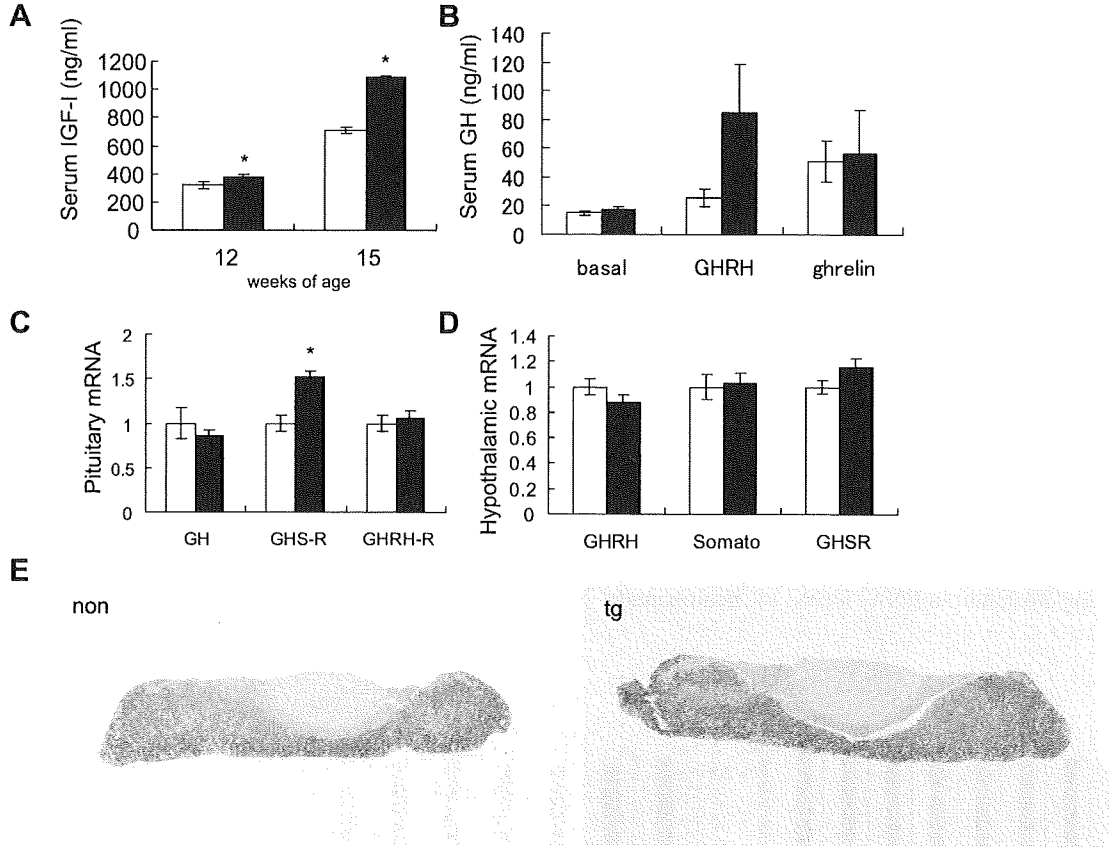

Fig. 5. GH-IGF-I axis in GP-Tag Tg mice. *A*: serum IGF-I levels in male GP-Tag Tg mice (black bars) and nontransgenic littermates (open bars); $n = 7–8$. *B*: serum GH levels at basal state and at 15 min after subcutaneous injection of GH-releasing hormone (GHRH) or ghrelin in male GP-Tag Tg mice (black bars) and nontransgenic littermates (open bars); $n = 8–13$. *C*: pituitary mRNA levels of GH, GHS-R, and GHRH-R in 15-wk-old male GP-Tag Tg mice (black bars) and nontransgenic littermates (open bars); $n = 7$. *D*: hypothalamic mRNA levels of GHRH, somatostatin (somato), and GHS-R in 15-wk-old male GP-Tag Tg mice (black bars) and nontransgenic littermates (open bars); $n = 7$. *E*: pituitary sections of 15-wk-old male Tg mice and non littermates immunostained with anti-GH antibody. $^*P < 0.05$ compared with non littermates.

(NS, $n = 7$; Fig. 5, *C* and *D*). Although plasma ghrelin level was elevated, pituitary GHS-R mRNA level was upregulated in GP-Tag Tg mice ($P < 0.05$, $n = 7$; Fig. 5*C*). We also examined pituitaries of 15-wk-old male GP-Tag Tg mice by immunohistochemical analysis. There were no obvious differences in somatotroph cell number or staining intensity of GH between GP-Tag Tg mice and nontransgenic littermates (Fig. 5*E*).

Glucose metabolism in GP-Tag Tg mice. Blood glucose levels of 15-wk-old male GP-Tag Tg mice were significantly higher than controls ($P < 0.05$, $n = 10$; Fig. 6*A*), although those of 9-wk-old male GP-Tag Tg mice were comparable with the controls (non-Tg vs. Tg: 96.0 ± 4.7 vs. 100.6 ± 4.7, $P = 0.51$, $n = 9$). Intraperitoneal glucose tolerance tests showed significantly higher blood glucose levels in 15-wk-old male GP-Tag Tg mice ($P < 0.05$, $n = 6–11$; Fig. 6*B*). To estimate the insulin sensitivity of GP-Tag Tg mice, we performed an insulin tolerance test. The blood glucose levels after insulin injection in 15-wk-old male GP-Tag Tg mice were suppressed to the same level of those in controls (NS, $n = 5–8$; Fig. 6*C*). Although basal insulin levels of 15-wk-old male GP-Tag Tg mice were not significantly different from those of control mice, those after glucose injection were significantly suppressed in GP-Tag Tg mice ($P < 0.05$, $n = 7–8$; Fig. 6*D*). Pancreatic mRNA and protein levels of insulin in GP-Tag Tg were comparable with those of nontransgenic littermates (NS, $n = 6–8$; Fig. 6, *E* and *F*).

DISCUSSION

In this study, we successfully established a mouse model of ghrelinoma, GP-Tag Tg mouse. GP-Tag Tg mice exhibited chronic elevation of circulating ghrelin with physiological regulation. The elevation of circulating ghrelin in GP-Tag Tg mice (~10-fold elevation) was much higher than that in bacterial artificial chromosome transgenic mice created by Bewick et al. (5) (only ~1.5-fold elevation). Nevertheless, the levels of circulating ghrelin in GP-Tag Tg mice can be considered to be within the physiological range since the highest level of plasma ghrelin observed in the anorexia patients is about seven times higher than those of normal controls (3). One may be confused by low ghrelin mRNA levels and low ghrelin production per milligram of tissue in the stomachs of GP-Tag Tg mice. In general, when the cell cycle progresses, endocrine cell produces far less amounts of hormone since the hormone production occurs mainly at the G_0/G_1 phase of the cell cycle. Since the hyperproliferaing ghrelin-producing cells in GP-Tag Tg mice were forced to proliferate by SV40 T-antigen, which suppresses RB protein and p53, promoting cell cycle progres-

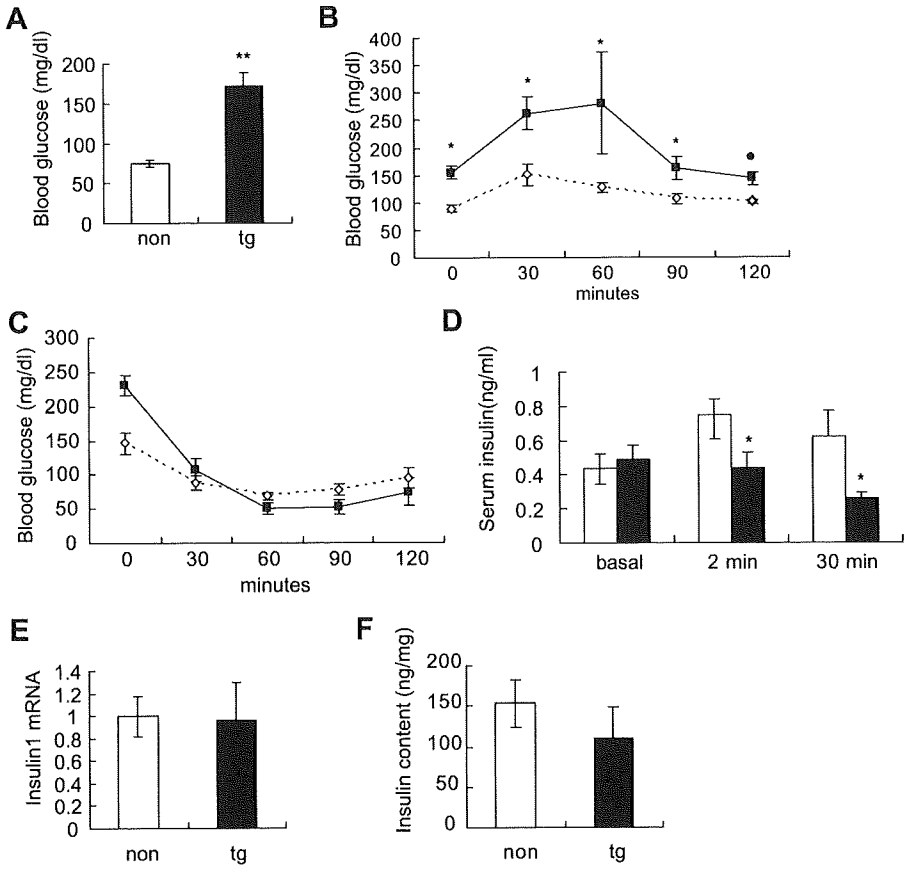

Fig. 6. Glucose metabolism in GP-Tag Tg mice. *A*: fasting blood glucose levels in 15-wk-old male Tg (black bar) and in non (open bar); n = 7–10. *B*: glucose tolerance tests in 15-wk-old male GP-Tag Tg mice (■) and in their nontransgenic littermates (◇); n = 6–11. *C*: insulin tolerance tests in male GP-Tag Tg mice (■) and in their nontransgenic littermates (◇); n = 5–8. *D*: serum insulin levels at basal, at 2 min, and at 30 min after intraperitoneal glucose injection in 15-wk-old male GP-Tag Tg mice (black bars) and in their nontransgenic littermates (open bars); n = 7–8. *E* and *F*: the mRNA (*E*) and the protein levels (*F*) of insulin in the pancreata of 15-wk-old male Tg mice (black bars) and in their non littermates (open bars); n = 6–8. $^{*}P < 0.05$, $^{**}P < 0.01$ compared with nontransgenic littermates.

sion, the amount of ghrelin production per cell was low. However, since the cell number was extremely increased, the net product by stomach was eventually elevated.

Several lines of evidence suggest that the GH-IGF-I axis is suppressed in the decreased GHS-R signaling state (28, 32). It has not yet been clear, however, whether chronic elevation of ghrelin within the physiological range could stimulate the GH-IGF-I axis. In this study, we found that adult GP-Tag Tg mice with elevated circulating ghrelin level showed elevated serum IGF-I level. Serum IGF-I level is regulated not only by GH but also by nutritional status. Malnutrition suppresses serum IGF-I level, whereas overnutrition elevates it (16). Since the nutritional state of GP-Tag Tg mice was poor because of decreased food intake, the elevated serum IGF-I levels in adult GP-Tag Tg mice are considered not to be due to overnutrition but to be due to activation of GH-IGF-I axis. Our findings indicate that chronic elevation of circulating ghrelin within the physiological range can activate the GH-IGF-I axis. As far as we know, this is the first report demonstrating that increased levels of circulating ghrelin within the physiological range can elevate serum IGF-I levels in rodent.

The GH-releasing action of ghrelin requires GHRH (11), and when coadministered, synergistic effects can be observed (13). Since GH responses to GHRH tended to be enhanced in adult GP-Tag Tg, the activation of the GH-IGF-I axis in GP-Tag Tg may be in part due to potentiation of the GH-releasing effect of GHRH. When the mRNA levels of components of GH regulation in pituitary and hypothalamus of GP-Tag Tg mice were investigated, an elevation of the pituitary GHS-R mRNA level was found. It is not clear whether this elevation of GHS-R mRNA in the pituitary contributes to the activated GH-IGF-I axis, since the GH response to ghrelin was not changed in GP-Tag Tg mice. At least these findings indicate that desensitization of GH secretion to ghrelin or downregulation of GHS-R did not occur by chronic elevation of circulating ghrelin in GP-Tag Tg mice.

Adult GP-Tag Tg mice exhibited high glucose level in the basal state and by the glucose tolerance test. Although insulin production was not decreased in the pancreata of GP-Tag Tg mice, insulin secretion after glucose load was significantly attenuated. Since the insulin sensitivity of GP-Tag Tg mice was not reduced, the glucose intorelance in GP-Tag Tg mice was due mainly to the decreased insulin secretion. Given that GP-Tag Tg mice have gastric tumors, there is a possibility that the glucose intorelance is due to the tumors. However, the glucose intolerance observed in malignancy is due mainly to insulin resistance (8, 15), which may be evoked by cytokines (22, 24, 27). Since the glucose intolerance of GP-Tag Tg mice was caused mainly by decreased insulin secretion, it seems not to be the case. It has been reported that acute injection of ghrelin induces suppression of insulin secretion in rodents and humans (6, 30). Our findings suggest that chronic elevation of circulating ghrelin within the physiological range leads to glucose intorelance by suppressing insulin secretion.

There have been several reports regarding ghrelin-producing tumors (9, 17, 36, 37). Most of the cases did not present

elevated plasma ghrelin levels except for a few cases. A malignant ghrelinoma case reported by Tsolakis et al. (36) showed elevated plasma ghrelin level. This patient maintained his weight despite progression of the tumor, a symptom that might be linked to the elevated ghrelin level. During the clinical course, he developed severe diabetes mellitus, which is consistent with the phenotype of GP-Tag Tg mice. GH and IGF-I levels were normal in this case. A pancreatic ghrelinoma case reported by Corbetta et al. (9) also showed normal GH and IGF-I levels despite elevated plasma ghrelin level. In contrast to these human ghrelinoma cases, GP-Tag Tg mice showed elevated IGF-I levels. The cause of the difference in the GH-IGF-I levels between our mice and these human ghrelinoma cases is unclear. Since the first case mentioned above was a malignant gastric ghrelinoma with liver metastasis, and the second case was of pancreatic origin, plasma ghrelin level might be elevated without any physiological regulation in these cases, although detailed plasma ghrelin level changes were not documented. Considering that the physiological regulation of ghrelin secretion was kept in GP-Tag Tg mice, the circadian rhythm may be needed for ghrelin to keep stimulating the GH-IGF-I axis. Indeed, several reports have shown that chronic treatment of ghrelin attenuates GH response both in vivo and in vitro (35, 39) and that in vitro treatment of pituitary with ghrelin results in decreased GHS-R mRNA levels (21). Further case studies will be required to reveal the relationship between plasma ghrelin levels and the GH-IGF-I axis in human ghrelinoma patients.

The limitation of this study is that the assessment of orexigenic action of ghrelin is difficult in this mouse model since stomach walls of GP-Tag Tg mice gradually become hypertrophic after 9 wk of age, which might affect the feeding behavior. Indeed, GP-Tag Tg mice exhibited decreased food intake and weight reduction despite the elevated plasma ghrelin levels. The hypothalamic mRNA levels of NPY and AgRP, which mediate the orexigenic action of ghrelin (7, 31), were not upregulated in GP-Tag Tg mice. There is a possibility that desensitization of GHS-R to chronic elevated ghrelin may be a cause of the lack of activation of these neurons besides the hypertrophy of the stomach wall. However, hypothalamic mRNA level of GHS-R was not changed. Furthermore, the food intake induced by acute ghrelin administration in GP-Tag Tg mice was comparable with control. These results may not support the idea of desensitization. Leptin and ghrelin have opposing effects on food intake. We examined whether plasma leptin levels of GP-Tag Tg mice were elevated as a compensation for the chronically elevated plasma ghrelin levels, which may cause anorexia. However, the leptin levels were decreased, provably reflecting the decreased fat mass of GP-Tag Tg mice.

In summary, we developed a mouse model of ghrelinoma, GP-Tag Tg mice, in which ghrelin concentrations were significantly elevated in adulthood. These GP-Tag Tg mice exhibited elevated IGF-I levels despite poor nutrition and glucose intolerance due to decreased insulin secretion. These characteristic features of this ghrelinoma mouse could be a guide to diagnose ghrelinoma.

ACKNOWLEDGMENTS

We thank Chieko Ishimoto and Chinami Shiraiwa for excellent technical assistance.

GRANTS

This study was supported by funds from the Ministry of Education, Culture, Sports, Science, and Technology of Japan and the Ministry of Health, Labour, and Welfare of Japan, a research grant from the Program for Promotion of Fundamental Studies in Health Sciences of the National Institute of Biomedical Innovation, and the Takeda Scientific Foundation in Japan.

REFERENCES

1. **Akamizu T, Shinomiya T, Irako T, Fukunaga M, Nakai Y, Kangawa K.** Separate measurement of plasma levels of acylated and desacyl ghrelin in healthy subjects using a new direct ELISA assay. *J Clin Endocrinol Metab* 90: 6–9, 2005.
2. **Ariyasu H, Takaya K, Iwakura H, Hosoda H, Akamizu T, Arai Y, Kangawa K, Nakao K.** Transgenic mice overexpressing des-acyl ghrelin show small phenotype. *Endocrinology* 146: 355–364, 2005.
3. **Ariyasu H, Takaya K, Tagami T, Ogawa Y, Hosoda K, Akamizu T, Suda M, Koh T, Natsui K, Toyooka S, Shirakami G, Usui T, Shimatsu A, Doi K, Hosoda H, Kojima M, Kangawa K, Nakao K.** Stomach is a major source of circulating ghrelin, and feeding state determines plasma ghrelin-like immunoreactivity levels in humans. *J Clin Endocrinol Metab* 86: 4753–4758, 2001.
4. **Asakawa A, Inui A, Fujimiya M, Sakamaki R, Shinfuku N, Ueta Y, Meguid MM, Kasuga M.** Stomach regulates energy balance via acylated ghrelin and desacyl ghrelin. *Gut* 54: 18–24, 2005.
5. **Bewick GA, Kent A, Campbell D, Patterson M, Ghatei MA, Bloom SR, Gardiner JV.** Mice with hyperghrelinemia are hyperphagic and glucose intolerant and have reduced leptin sensitivity. *Diabetes* 58: 840–846, 2009.
6. **Broglio F, Arvat E, Benso A, Gottero C, Muccioli G, Papotti M, van der Lely AJ, Deghenghi R, Ghigo E.** Ghrelin, a natural GH secretagogue produced by the stomach, induces hyperglycemia and reduces insulin secretion in humans. *J Clin Endocrinol Metab* 86: 5083–5086, 2001.
7. **Chen HY, Trumbauer ME, Chen AS, Weingarth DT, Adams JR, Frazier EG, Shen Z, Marsh DJ, Feighner SD, Guan XM, Ye Z, Nargund RP, Smith RG, Van der Ploeg LH, Howard AD, MacNeil DJ, Qian S.** Orexigenic action of peripheral ghrelin is mediated by neuropeptide Y and agouti-related protein. *Endocrinology* 145: 2607–2612, 2004.
8. **Copeland GP, Leinster SJ, Davis JC, Hipkin LJ.** Insulin resistance in patients with colorectal cancer. *Br J Surg* 74: 1031–1035, 1987.
9. **Corbetta S, Peracchi M, Cappiello V, Lania A, Lauri E, Vago L, Beck-Peccoz P, Spada A.** Circulating ghrelin levels in patients with pancreatic and gastrointestinal neuroendocrine tumors: identification of one pancreatic ghrelinoma. *J Clin Endocrinol Metab* 88: 3117–3120, 2003.
10. **Date Y, Kojima M, Hosoda H, Sawaguchi A, Mondal MS, Suganuma T, Matsukura S, Kangawa K, Nakazato M.** Ghrelin, a novel growth hormone-releasing acylated peptide, is synthesized in a distinct endocrine cell type in the gastrointestinal tracts of rats and humans. *Endocrinology* 141: 4255–4261, 2000.
11. **Dimaraki EV, Jaffe CA.** Role of endogenous ghrelin in growth hormone secretion, appetite regulation and metabolism. *Rev Endocr Metab Disord* 7: 237–249, 2006.
12. **Gutierrez JA, Solenberg PJ, Perkins DR, Willency JA, Knierman MD, Jin Z, Witcher DR, Luo S, Onyia JE, Hale JE.** Ghrelin octanoylation mediated by an orphan lipid transferase. *Proc Natl Acad Sci USA* 105: 6320–6325, 2008.
13. **Hataya Y, Akamizu T, Takaya K, Kanamoto N, Ariyasu H, Saijo M, Moriyama K, Shimatsu A, Kojima M, Kangawa K, Nakao K.** A low dose of ghrelin stimulates growth hormone (GH) release synergistically with GH-releasing hormone in humans. *J Clin Endocrinol Metab* 86: 4552, 2001.
14. **Hosoda H, Kojima M, Matsuo H, Kangawa K.** Ghrelin and des-acyl ghrelin: two major forms of rat ghrelin peptide in gastrointestinal tissue. *Biochem Biophys Res Commun* 279: 909–913, 2000.
15. **Isaksson B, Strommer L, Friess H, Buchler MW, Herrington MK, Wang F, Zierath JR, Wallberg-Henriksson H, Larsson J, Permert J.** Impaired insulin action on phosphatidylinositol 3-kinase activity and glucose transport in skeletal muscle of pancreatic cancer patients. *Pancreas* 26: 173–177, 2003.
16. **Iwakura H, Akamizu T, Ariyasu H, Irako T, Hosoda K, Nakao K, Kangawa K.** Effects of ghrelin administration on decreased growth hormone status in obese animals. *Am J Physiol Endocrinol Metab* 293: E819–E825, 2007.

17. **Iwakura H, Hosoda K, Doi R, Komoto I, Nishimura H, Son C, Fujikura J, Tomita T, Takaya K, Ogawa Y, Hayashi T, Inoue G, Akamizu T, Hosoda H, Kojima M, Kangawa K, Imamura M, Nakao K.** Ghrelin expression in islet cell tumors: augmented expression of ghrelin in a case of glucagonoma with multiple endocrine neoplasm type I. *J Clin Endocrinol Metab* 87: 4885–4888, 2002.
18. **Iwakura H, Hosoda K, Son C, Fujikura J, Tomita T, Noguchi M, Ariyasu H, Takaya K, Masuzaki H, Ogawa Y, Hayashi T, Inoue G, Akamizu T, Hosoda H, Kojima M, Itoh H, Toyokuni S, Kangawa K, Nakao K.** Analysis of rat insulin II promoter-ghrelin transgenic mice and rat glucagon promoter-ghrelin transgenic mice. *J Biol Chem* 280: 15247–15256, 2005.
19. **Kanamoto N, Akamizu T, Tagami T, Hataya Y, Moriyama K, Takaya K, Hosoda H, Kojima M, Kangawa K, Nakao K.** Genomic structure and characterization of the 5′-flanking region of the human ghrelin gene. *Endocrinology* 145: 4144–4153, 2004.
20. **Kojima M, Hosoda H, Date Y, Nakazato M, Matsuo H, Kangawa K.** Ghrelin is a growth-hormone-releasing acylated peptide from stomach. *Nature* 402: 656–660, 1999.
21. **Luque RM, Kineman RD, Park S, Peng XD, Gracia-Navarro F, Castano JP, Malagon MM.** Homologous and heterologous regulation of pituitary receptors for ghrelin and growth hormone-releasing hormone. *Endocrinology* 145: 3182–3189, 2004.
22. **Makino T, Noguchi Y, Yoshikawa T, Doi C, Nomura K.** Circulating interleukin 6 concentrations and insulin resistance in patients with cancer. *Br J Surg* 85: 1658–1662, 1998.
23. **Masuda Y, Tanaka T, Inomata N, Ohnuma N, Tanaka S, Itoh Z, Hosoda H, Kojima M, Kangawa K.** Ghrelin stimulates gastric acid secretion and motility in rats. *Biochem Biophys Res Commun* 276: 905–908, 2000.
24. **McCall JL, Tuckey JA, Parry BR.** Serum tumour necrosis factor alpha and insulin resistance in gastrointestinal cancer. *Br J Surg* 79: 1361–1363, 1992.
25. **Nagaya N, Kojima M, Uematsu M, Yamagishi M, Hosoda H, Oya H, Hayashi Y, Kangawa K.** Hemodynamic and hormonal effects of human ghrelin in healthy volunteers. *Am J Physiol Regul Integr Comp Physiol* 280: R1483–R1487, 2001.
26. **Nakazato M, Murakami N, Date Y, Kojima M, Matsuo H, Kangawa K, Matsukura S.** A role for ghrelin in the central regulation of feeding. *Nature* 409: 194–198, 2001.
27. **Noguchi Y, Yoshikawa T, Marat D, Doi C, Makino T, Fukuzawa K, Tsuburaya A, Satoh S, Ito T, Mitsuse S.** Insulin resistance in cancer patients is associated with enhanced tumor necrosis factor-alpha expression in skeletal muscle. *Biochem Biophys Res Commun* 253: 887–892, 1998.
28. **Pantel J, Legendre M, Cabrol S, Hilal L, Hajaji Y, Morisset S, Nivot S, Vie-Luton MP, Grouselle D, de Kerdanet M, Kadiri A, Epelbaum J, Le Bouc Y, Amselem S.** Loss of constitutive activity of the growth hormone secretagogue receptor in familial short stature. *J Clin Invest* 116: 760–768, 2006.
29. **Reed JA, Benoit SC, Pfluger PT, Tschöp MH, D'Alessio DA, Seeley RJ.** Mice with chronically increased circulating ghrelin develop age-related glucose intolerance. *Am J Physiol Endocrinol Metab* 294: E752–E760, 2008.
30. **Reimer MK, Pacini G, Ahren B.** Dose-dependent inhibition by ghrelin of insulin secretion in the mouse. *Endocrinology* 144: 916–921, 2003.
31. **Shintani M, Ogawa Y, Ebihara K, Aizawa-Abe M, Miyanaga F, Takaya K, Hayashi T, Inoue G, Hosoda K, Kojima M, Kangawa K, Nakao K.** Ghrelin, an endogenous growth hormone secretagogue, is a novel orexigenic peptide that antagonizes leptin action through the activation of hypothalamic neuropeptide Y/Y1 receptor pathway. *Diabetes* 50: 227–232, 2001.
32. **Shuto Y, Shibasaki T, Otagiri A, Kuriyama H, Ohata H, Tamura H, Kamegai J, Sugihara H, Oikawa S, Wakabayashi I.** Hypothalamic growth hormone secretagogue receptor regulates growth hormone secretion, feeding, and adiposity. *J Clin Invest* 109: 1429–1436, 2002.
33. **Tack J, Depoortere I, Bisschops R, Delporte C, Coulie B, Meulemans A, Janssens J, Peeters T.** Influence of ghrelin on interdigestive gastrointestinal motility in humans. *Gut* 55: 327–333, 2006.
34. **Takaya K, Ariyasu H, Kanamoto N, Iwakura H, Yoshimoto A, Harada M, Mori K, Komatsu Y, Usui T, Shimatsu A, Ogawa Y, Hosoda K, Akamizu T, Kojima M, Kangawa K, Nakao K.** Ghrelin strongly stimulates growth hormone release in humans. *J Clin Endocrinol Metab* 85: 4908–4911, 2000.
35. **Thompson NM, Davies JS, Mode A, Houston PA, Wells T.** Pattern-dependent suppression of growth hormone (GH) pulsatility by ghrelin and GH-releasing peptide-6 in moderately GH-deficient rats. *Endocrinology* 144: 4859–4867, 2003.
36. **Tsolakis AV, Portela-Gomes GM, Stridsberg M, Grimelius L, Sundin A, Eriksson BK, Oberg KE, Janson ET.** Malignant gastric ghrelinoma with hyperghrelinemia. *J Clin Endocrinol Metab* 89: 3739–3744, 2004.
37. **Volante M, Allia E, Gugliotta P, Funaro A, Broglio F, Deghenghi R, Muccioli G, Ghigo E, Papotti M.** Expression of ghrelin and of the GH secretagogue receptor by pancreatic islet cells and related endocrine tumors. *J Clin Endocrinol Metab* 87: 1300–1308, 2002.
38. **Wei W, Qi X, Reed J, Ceci J, Wang HQ, Wang G, Englander EW, Greeley GH Jr.** Effect of chronic hyperghrelinemia on ingestive action of ghrelin. *Am J Physiol Regul Integr Comp Physiol* 290: R803–R808, 2006.
39. **Yamazaki M, Nakamura K, Kobayashi H, Matsubara M, Hayashi Y, Kangawa K, Sakai T.** Regulational effect of ghrelin on growth hormone secretion from perifused rat anterior pituitary cells. *J Neuroendocrinol* 14: 156–162, 2002.
40. **Yang J, Brown MS, Liang G, Grishin NV, Goldstein JL.** Identification of the acyltransferase that octanoylates ghrelin, an appetite-stimulating peptide hormone. *Cell* 132: 387–396, 2008.
41. **Zhang W, Chai B, Li JY, Wang H, Mulholland MW.** Effect of des-acyl ghrelin on adiposity and glucose metabolism. *Endocrinology* 149: 4710–4716, 2008.

p300 Plays a Critical Role in Maintaining Cardiac Mitochondrial Function and Cell Survival in Postnatal Hearts

Yasuaki Nakagawa, Koichiro Kuwahara, Genzo Takemura, Masaharu Akao, Masashi Kato, Yuji Arai, Makoto Takano, Masaki Harada, Masao Murakami, Michio Nakanishi, Satoru Usami, Shinji Yasuno, Hideyuki Kinoshita, Masataka Fujiwara, Kenji Ueshima, Kazuwa Nakao

Rationale: It is known that the transcriptional coactivator p300 is crucially involved in the differentiation and growth of cardiac myocytes during development. However, the physiological function of p300 in the postnatal hearts remains to be characterized.

Objective: We have now investigated the physiological function of p300 in adult hearts.

Methods and Results: We analyzed transgenic mice exhibiting cardiac-specific overexpression of a dominant-negative p300 mutant lacking the C/H3 domain (p300ΔC/H3 transgenic [TG] mice). p300ΔC/H3 significantly inhibited p300-induced activation of GATA- and myocyte enhancer factor 2–dependent promoters in cultured ventricular myocytes, and p300ΔC/H3-TG mice showed cardiac dysfunction that was lethal by 20 weeks of age. The numbers of mitochondria in p300ΔC/H3-TG myocytes were markedly increased, but the mitochondria were diminished in size. Moreover, cardiac mitochondrial gene expression, mitochondrial membrane potential and ATP contents were all significantly disrupted in p300ΔC/H3-TG hearts, suggesting that mitochondrial dysfunction contributes to the progression of the observed cardiomyopathy. Transcription of peroxisome proliferator-activated receptor γ coactivator (PGC)-1α, a master regulator of mitochondrial gene expression, and its target genes was significantly downregulated in p300ΔC/H3-TG mice, and p300ΔC/H3 directly repressed myocyte enhancer factor 2C-dependent PGC-1α promoter activity and disrupted the transcriptional activity of PGC-1α in cultured ventricular myocytes. In addition, myocytes showing features of autophagy were observed in p300ΔC/H3-TG hearts.

Conclusions: Collectively, our findings suggest that p300 is essential for the maintenance of mitochondrial integrity and for myocyte survival in the postnatal left ventricular myocardium. (*Circ Res.* 2009;105:746-754.)

Key Words: mitochondrial function ■ autophagy ■ transcription ■ cardiac dysfunction

The transcriptional coactivator p300 interacts directly with components of the basal transcriptional apparatus and various enhancer-binding proteins, thereby modulating enhancer-mediated transcription.[1,2] Several lines of evidence suggest that p300 plays a critical role in the differentiation and growth of cardiac myocytes during development. For example, mice lacking a functional p300 gene die in utero, between embryonic days 9 and 11.5, because of disruption of cardiac muscle differentiation and trabeculation.[3] Within the myocardium, p300 serves as a coactivator of several transcription factors enriched in cardiac tissue, including GATA-4, myocyte enhancer factor (MEF)2, and serum response factor, and is required for these factors to exhibit their full transcriptional activities.[4–6] Notably, these molecules are also known to function as hypertrophy-responsive transcription factors during the pathogenesis of cardiac hypertrophy and heart failure in adults, and transgenic mice expressing p300 under the control of the cardiac-specific α-myosin heavy chain (MHC) promoter exhibit eccentric cardiac hypertrophy and increased mortality,[7] whereas cardiac-specific overexpression of p300 exacerbates adverse cardiac remodeling after myocardial infarction.[8] These findings imply that in some cases a therapeutic benefit may be obtained through inhibition of p300.[9] On the other hand, p300 appears to be essential for normal cardiac development[3,10] and important for cardiac myocyte survival under some conditions.[11]

Original received April 4, 2008; resubmission received July 28, 2009; revised resubmission received August 24, 2009; accepted August 25, 2009.

From the Department of Medicine and Clinical Science (Y.N., K.K., M.H., M.M., M.N., S.U., S.Y., H.K., M.F., K.N.), Department of Cardiovascular Medicine (M.A., M.K.), and EBM Research Center (K.U.), Kyoto University Graduate School of Medicine; Department of Cardiology and Respirology, Regeneration and Advanced Medical Sciences (G.T.), Graduate School of Medicine, Gifu University; Department of Bioscience (Y.A.), National Cardiovascular Center Research Institute, Suita; and Department of Biophysics (M.T.), Jichi Medical School, Shimotsuke, Japan.

Correspondence to Koichiro Kuwahara, Department of Medicine and Clinical Science, Kyoto University Graduate School of Medicine, 54, Shogoin-Kawara-cho, Sakyo-ku, Kyoto 606-8507, Japan. E-mail kuwa@kuhp.kyoto-u.ac.jp

Circulation Research is available at http://circres.ahajournals.org

DOI: 10.1161/CIRCRESAHA.109.206037

Consequently, inhibiting the activity of p300 could have adverse effects on the adult heart.

Peroxisome proliferator-activated receptor (PPAR)γ coactivator (PGC)-1α,[12] estrogen-related receptor (ERR)α,[13] and PPARα[14] are 3 mediators recently shown to regulate mitochondrial biogenesis and gene expression.[15] PGC-1α was cloned based on its ability to interact with PPARγ[16] and appears to be a critical regulator involved in the control of cardiac mitochondrial function in response to energy demands.[12] ERRα reportedly acts as an effector of PGC-1α and is an important regulator of genes involved in oxidative phosphorylation and mitochondrial biogenesis.[17] Furthermore, PPARα was shown to regulate expression of genes involved in mitochondrial fatty acid oxidation.[14] It is known that p300 forms complexes with PGC-1α and PPARα,[18–20] but the precise function of p300 in mitochondrial gene expression and function remains unclear.

Our aim in the present study was to examine the physiological function of p300 in the postnatal heart. To accomplish that, we developed a transgenic (TG) mouse that overexpresses a dominant-negative p300 mutant lacking the C/H3 domain (p300ΔC/H3) under the control of the cardiac-specific α-MHC promoter. Notably, these p300ΔC/H3 transgenic (p300ΔC/H3-TG) mice showed severe cardiomyopathy and died prematurely, and our findings demonstrate that p300 is essential for the maintenance of mitochondrial integrity and for the survival of cardiac myocytes in the postnatal heart.

Non-standard Abbreviations and Acronyms	
ANP	atrial natriuretic peptide
BNP	brain natriuretic peptide
ERRα	estrogen-related receptor α
H&E	hematoxylin/eosin
LC3	microtubule-associated protein 1 light chain 3
LV	left ventricular
MEF2	myocyte enhancer factor 2
MHC	myosin heavy chain
PGC-1α	peroxisome proliferator-activated receptor γ coactivator-1α
PPAR	peroxisome proliferator-activated receptor
SERCA2	sarcoplasmic/endoplasmic reticulum calcium ATPase 2
SRPK3	serine/arginine-rich protein–specific kinase 3
TG	transgenic
TMRE	tetramethylrhodamine ethyl ester
WT	wild type

Methods

Plasmid Constructs

A fragment containing full-length wild-type (WT) p300 or p300ΔC/H3, in which the C/H3 domain was deleted, was inserted into the pCMVβ. Constructs containing the luciferase gene driven by the −452 bp of the proximal enhancer–promoter region of the atrial natriuretic peptide (ANP) gene (−452hANPluc) or by the −1812 bp of the enhancer-promoter region of the brain natriuretic peptide (BNP) gene (−1812hBNPluc) were described previously.[21,22] Luciferase reporter genes driven by the promoter region of the PCG1α gene, tandem GATA sites (GATA-luc), and tandem MEF2 sites (3xMEF2-luc) were kindly provided by M. D. Schneider (Baylor College of Medicine, Houston, Tex), R. S. Viger (University Laval, Ontario, Canada), and E. N. Olson (University of Texas Southwestern Medical Center, Dallas, Tex), respectively. A luciferase reporter gene driven by multiple PPAR response element sites and an expression vector encoding ERRα were kindly provided by D. P. Kelly (Washington University, St Louis, Mo).

Cell Culture, Transfection, and Luciferase Assay

Neonatal rat ventricular myocytes were prepared and transiently transfected by electroporation as described previously.[23,24]

Western Blotting Analysis

To evaluate autophagy, we used an antimicrotubule-associated protein 1 light chain 3 (LC3) antibody kindly provided by N. Mizushima (Tokyo Medical and Dental University, Japan)[25,26] and an anti–cathepsin D antibody (Santa Cruz Biotechnology).

Tetramethylrhodamine Ethyl Ester Staining of Isolated Adult Mouse Cardiomyocytes and Whole Hearts Ex Vivo

Isolated ventricular myocytes were suspended in DMEM supplemented with 10 mmol/L HEPES and plated in 6-well dishes. Tetramethylrhodamine ethyl ester (TMRE) (100 nmol/L; Molecular Probes, Eugene) was then added to the medium for 30 minutes, after which the intensity of TMRE fluorescence was evaluated using confocal microscopy.

For TMRE staining of whole hearts ex vivo, we analyzed Langendorff-perfused mouse hearts using a modification of the Langendorff method previously described for use with rat hearts.[27]

Statistical Analysis

Data are presented as means±SEM. Unpaired *t* tests were used for comparisons between 2 groups, and ANOVA with post hoc Fisher's tests was used for comparison among groups. Values of $P<0.05$ were considered significant.

An expanded Methods section is available in the Online Data Supplement at http://circres.ahajournals.org.

Results

p300ΔC/H3 Inhibits the Activities of Cardiac Transcription Factors and Cardiac Gene Transcription in a Dominant-Negative Fashion

A well-conserved C/H3 domain is necessary for the interaction of p300 with multiple DNA-binding factors,[4,28–30] and p300 lacking its C/H3 domain reportedly acts as a dominant-negative mutant.[2] With that in mind, we initially tested whether a p300 C/H3 deletion mutant (p300ΔC/H3) would exert a dominant-negative effect on the cardiac-enriched transcription factors MEF2 and GATA4, both of which are known to functionally interact with p300.[4,28] p300ΔC/H3 dose-dependently inhibited GATA 4- and MEF 2-induced transcriptional activation of the reporter genes (Figure 1A and 1B), and also inhibited p300-induced enhancement of GATA4- and MEF2-mediated transcription, confirming its dominant-negative effect (Figure 1C and 1D).

To examine the effect of p300ΔC/H3 on the expression of cardiac genes, we cotransfected cultured rat neonatal ventricular myocytes with p300ΔC/H3 and −452hANPLuc or −1812hBNPLuc, and found that p300ΔC/H3 dose-dependently inhibited the activities of both −452hANPLuc and−1812hBNPLuc (Figure 1E and 1F), as well as GATA4-

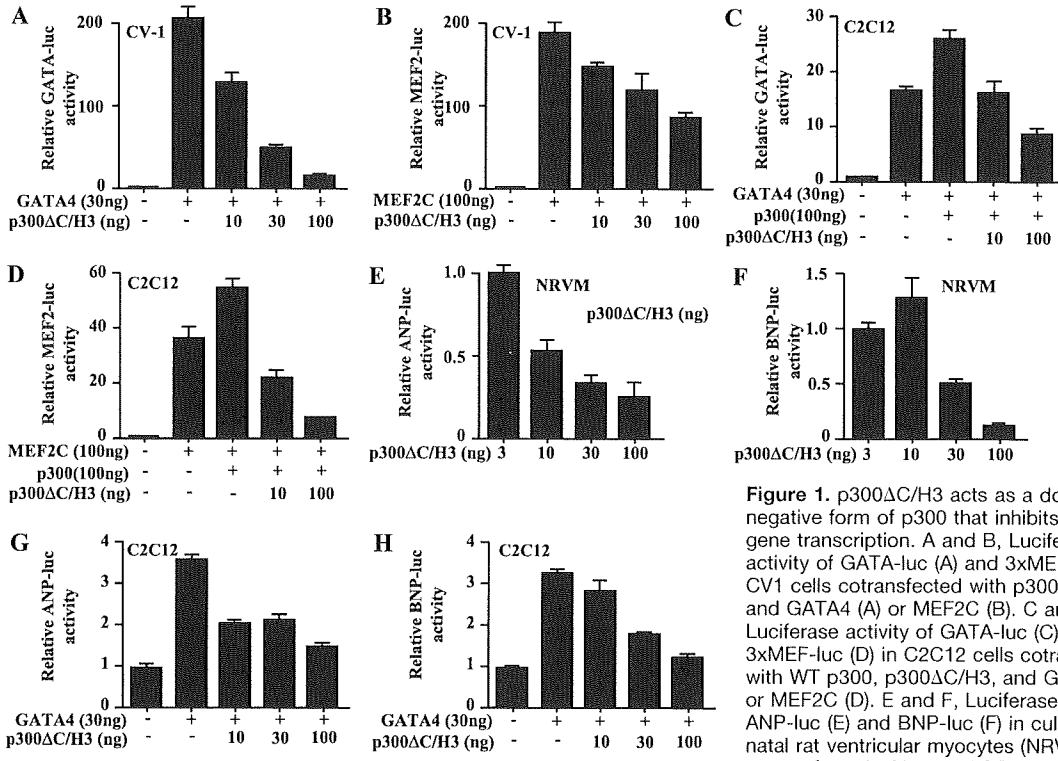

Figure 1. p300ΔC/H3 acts as a dominant negative form of p300 that inhibits cardiac gene transcription. A and B, Luciferase activity of GATA-luc (A) and 3xMEF-luc (B) in CV1 cells cotransfected with p300ΔC/H3 and GATA4 (A) or MEF2C (B). C and D, Luciferase activity of GATA-luc (C) and 3xMEF-luc (D) in C2C12 cells cotransfected with WT p300, p300ΔC/H3, and GATA4 (C) or MEF2C (D). E and F, Luciferase activity of ANP-luc (E) and BNP-luc (F) in cultured neonatal rat ventricular myocytes (NRVM) cotransfected with p300ΔC/H3. G and H, Luciferase activity of ANP-luc (G) and BNP-luc (H) in C2C12 cells cotransfected with GATA4 and p300ΔC/H3. In all experiments, luciferase activities in cells transfected with the reporter construct alone were assigned a value of 1.0. Bars represent means±SEM.

induced activation of −452hANPLuc and −1812hBNPLuc in C2C12 cells (Figure 1G and 1H).

Cardiac Overexpression of p300ΔC/H3 Causes Heart Failure and Premature Death

Having confirmed the dominant-negative effect of p300ΔC/H3, we sought to evaluate the physiological function of p300 in adult heart using p300ΔC/H3-TG mice, in which p300ΔC/H3 was expressed under the control of the cardiac-specific αMHC promoter (Figure 2A). We obtained and investigated 2 independently derived p300ΔC/H3-TG founders (TG1 and TG2). The data obtained from TG1 were essentially the same as those obtained from TG2 shown in Online Figure I (A through H) and are presented below. Expression of the protein encoded by the transgene was confirmed by Western blotting with an anti-hemagglutinin tag antibody (Figure 2B). Moreover, Western blotting with antibodies recognizing both WT mouse p300 and mutant human p300ΔC/H3 showed that the level of p300ΔC/H3 expression was 1.9-fold higher than that of endogenous p300 (Figure 2C).

p300ΔC/H3-TG mice appeared normal at birth, but by 12 weeks after birth, their survival rate was significantly lower than that of WT mice (survival rate at 12 weeks of age: WT [n=40], 100%; TG [n=28], 71%; Figure 2D), and almost all had died by 20 weeks of age (survival rate at 20 weeks of age: WT [n=40], 100%; TG [n=28], 3.5%; Figure 2D). The survival rate among p300ΔC/H3-TG mice was also much lower than that among TG mice overexpressing exogenous WT p300 in their hearts, which showed 76% survival at 42 weeks of age.[7] At 12 weeks of age, the hearts of p300ΔC/H3-TG mice were much larger than those of WT mice (Figure 2E, 2F and 2G). Likewise, the lung weight/body weight ratios were significantly higher in p300ΔC/H3-TG mice (Figure 2H). Echocardiographic analysis revealed the ejection fraction to be significantly reduced and the left ventricular (LV) end-systolic diameter to be significantly increased in p300ΔC/H3-TG mice (Table). In another transgenic mouse, TG2, which expressed the transgene at a lower level than TG1, we found similar but milder LV dysfunction and dilatation (Online Figure I, A through F). Hemodynamic analysis of 12-week-old p300ΔC/H3-TG mice also indicated LV dysfunction, as reflected by markedly elevated LV end-diastolic pressure and significant depression of both the maximal and minimal rates of LV pressure development (dP/dt-max and dP/dt-min, respectively) (Table).

When we then used real-time PCR to examine the expression of cardiac stress markers in p300ΔC/H3-TG mice, we found that expression of both ANP and BNP was markedly upregulated, and expression of sarcoplasmic/endoplasmic reticular calcium ATPase (SERCA)2 was significantly downregulated in p300ΔC/H3-TG hearts (Figure 2I through 2K; Online Figure I, G).[31,32] Although p300ΔC/H3 inhibited ANP and BNP gene transcription in cultured cardiac myocytes, this suggests that endogenous p300 is

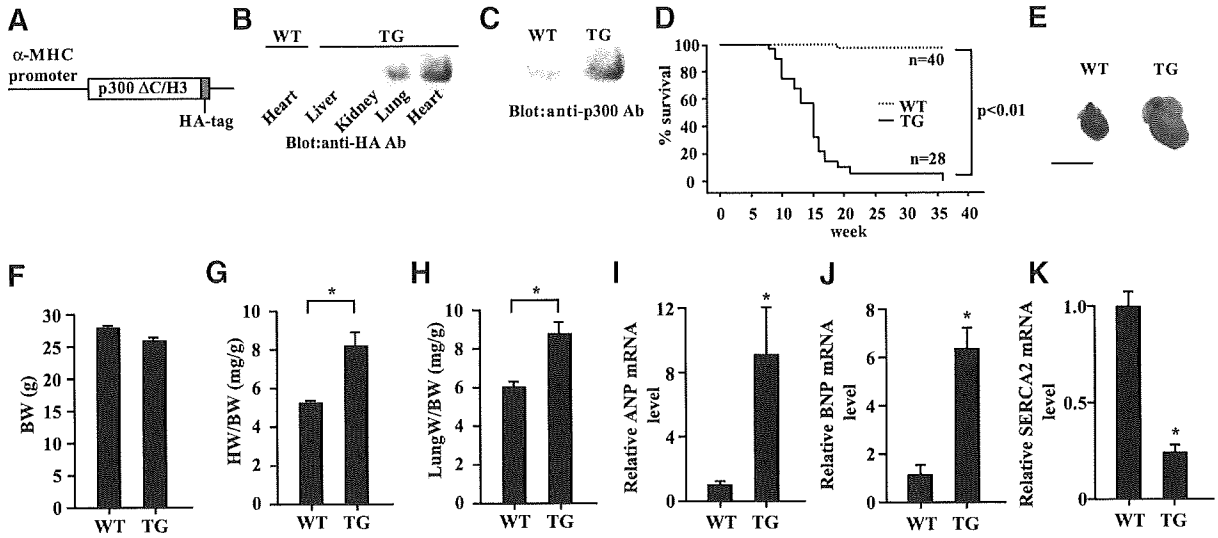

Figure 2. Premature death and cardiomyopathy in p300ΔC/H3-TG mice. A, Schematic representation of the construct for the αMHC-p300ΔC/H3 transgene. B, Western blot analysis of p300ΔC/H3 in the indicated tissue was performed using anti-hemagglutinin (HA) antibody. C, Western blot analysis of WT mouse p300 and mutant human p300ΔC/H3 in the heart was performed using an antip300 antibody able to detect both WT mouse p300 and mutant human p300ΔC/H3. D, Kaplan–Meier survival analysis of p300ΔC/H3-TG and WT mice showing a significant difference in survival rates. E, Gross appearance of hearts from 12-week-old p300ΔC/H3-TG and WT mice. Scale bars=10 mm. F through H, Body weights (BW) (F), heart weight/body weight (HW/BW) ratios (G), and lung weight/body weight ratios (LuW/BW) (H) in 12-week-old p300ΔC/H3-TG and WT mice. *$P<0.05$. I through K, Relative levels of ANP (I), BNP (J), and SERCA2 (K) mRNA quantified by real-time RT-PCR in ventricles of WT and p300ΔC/H3-TG hearts. *$P<0.05$ vs WT. Relative mRNA levels in WT were assigned a value of 1.0. Bars represent means±SEM.

not required for pathological induction of these fetal cardiac genes in adult hearts.

Histological examination of cross-sections confirmed enlargement of the atrial and ventricular chambers in 12-week-old p300ΔC/H3-TG hearts (Figure 3A, 3B, 3C, and 3D). At higher magnification, hematoxylin/eosin (H&E)-stained ventricular myocytes from p300ΔC/H3-TG hearts were highly variable in size (Figure 3E and 3F). In addition, Sirius red staining revealed the presence of significant interstitial fibrosis in p300ΔC/H3-TG ventricles (Figure 3G and 3H), whereas electron microscopic examination revealed vacuolization of the ventricular myocytes and myofibrillar degeneration, features typical of human cardiomyopathy (Figure 3I). We also performed oil-O-red staining to compare the lipid droplets in the ventricular myocardia of WT and p300ΔC/H3-TG mice and found there to be no difference between the 2 genotypes (data not shown).

Table. Echocardiographic and Hemodynamic Analysis in 12-Week-Old WT and p300ΔC/H3-TG Mice

Analysis	Wild Type	Transgenic	*P*
Echographic data			
N	8	11	
LVDd (mm)	4.24±0.63	5.26±0.11	<0.0001
LVDs (mm)	3.05±0.07	4.61±0.14	<0.0001
IVST (mm)	0.63±0.04	0.56±0.04	0.202
PWT (mm)	0.59±0.03	0.56±0.41	0.555
FS (%)	29.88±0.93	12.82±1.20	<0.0001
EF (%)	65.50±1.48	33.09±2.59	<0.0001
Hemodynamic data			
N	3	3	
LVSP (mm Hg)	100.07±0.87	86.67±8.75	0.202
LVEDP (mm Hg)	5.87±0.353	2.93±3.733	0.133
dP/dt (mm Hg/sec)	4913.33±96.84	3768.00±322.86	0.0274
−dP/dt (mm Hg/sec)	−5146.67±327.48	−2853.33±233.33	0.0047
HR (bpm)	581.67±18.33	481.67±42.33	0.0242

Values are means±SEM. dP/dt indicates first derivative of pressure; EF, ejection fraction; FS, fractional shortening; HR, heart rate; IVST, interventricular septal thickness; LVEDP, left ventricular end diastolic pressure; LVDd, left ventricular end diastolic dimension; LVDs, left ventricular end systolic diameter; LVSP, left ventricular systolic pressure; PWT, posterior wall thickness.

p300ΔC/H3 Directly Inhibits the Expression and Function of PGC-1α

Electron microscopic examination also revealed that the numbers of mitochondria were dramatically increased in p300ΔC/H3-TG myocytes, but that they were much smaller in size than those in WT myocytes (Figure 3I). This prompted us to assess the expression and function of mitochondrial genes in p300ΔC/H3-TG mice. Using quantitative real-time RT-PCR, we evaluated the transcription of genes related to mitochondrial fatty acid oxidation and mitochondrial replication. Expression of nuclear respiratory factor (NRF)1 and mitochondrial transcription factor A mRNAs was significantly downregulated in p300ΔC/H3-TG hearts, as compared to WT hearts (Figure 4A). Expression of genes involved in fatty acid oxidation, including carnitine palmitoyltransferase-I and -II and medium- and long-chain acyl-coenzyme A

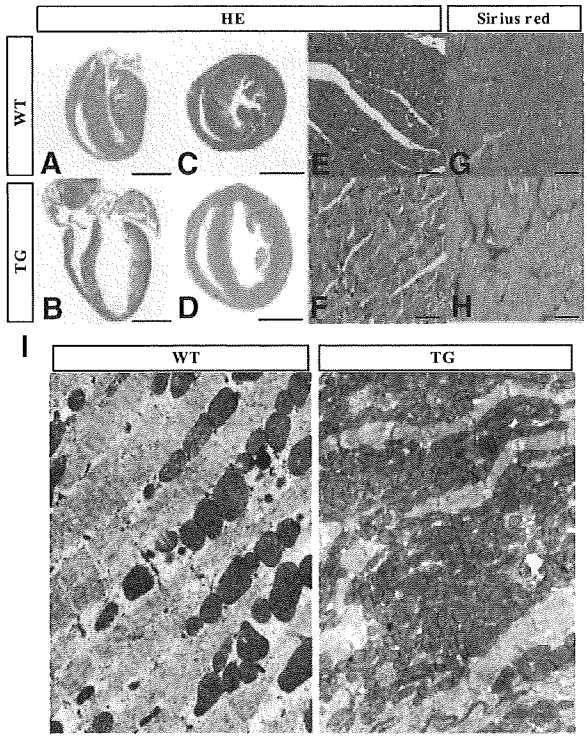

Figure 3. Pathological changes in p300ΔC/H3-TG hearts. A through H, Histological analysis of hearts from 12-week-old p300ΔC/H3-TG and WT mice. A through D, Hearts from WT (A and C) and p300ΔC/H3-TG (B and D) mice were sectioned longitudinally (A and B) or coronally (C and D) and stained with H&E. Scale bars=2.5 mm. E through H, Higher magnification of histological sections of WT (E and G) and p300ΔC/H3-TG (F and H) hearts stained with H&E (E and F) or Sirius red (G and H). Scale bars=50 μm. I, Transmission electron micrographs of cardiac myocytes from 12-week-old WT (left) and p300ΔC/H3-TG (right) hearts.

dehydrogenase, was also diminished in P300ΔC/H3-TG hearts (Figure 4A; Online Figure I, H). Given these reductions in mitochondrial gene expression in p300ΔC/H3-TG hearts, we also evaluated the expression of genes encoding PGC-1α, ERRα, and PPARα, 3 mediators thought to be involved in regulating mitochondrial gene expression. As shown in Figure 4B and Online Figure I (H), expression of all 3 was significantly downregulated in p300ΔC/H3-TG mice.

It was recently reported that PGC-1α induces the expression of ERRα and then interacts with the expressed protein, enabling it to activate transcription.[17] In addition, ERRα reportedly activates PPARα gene expression by directly binding to the PPARα promoter.[13] Therefore, to determine whether p300ΔC/H3 directly inhibits transcription of PGC-1α, the upstream activator of ERRα and PPARα, we carried out reporter assays using a PGC-1α promoter-luciferase reporter gene. In neonatal rat ventricular myocytes, p300ΔC/H3 significantly and dose-dependently inhibited the activity of the PGC-1α promoter (Figure 4C).

Because MEF2, a muscle-enriched transcriptional activator that interacts with p300, was previously shown to regulate PGC-1α promoter activity,[33,34] we next tested the effect of p300ΔC/H3 on MEF2C-inducible PGC-1α promoter activity in CV1 cells. We found that MEF2C-induced PGC-1α promoter activity was significantly inhibited by p300ΔC/H3 (Figure 4D), suggesting that p300ΔC/H3 directly inhibits PGC-1α gene expression in p300ΔC/H3-TG hearts. The mRNA expression of serine/arginine-rich protein–specific kinase (SRPK)3, another MEF2 target gene, was also significantly downregulated in p300ΔC/H3-TG hearts (Figure 4E). In addition, because p300 reportedly acts as a coactivator of PGC-1α and ERRα, we also tested whether p300ΔC/H3 directly inhibits PGC-1α-mediated activation of ERRα, which would in turn inhibit PPARα gene expression. That p300ΔC/H3 significantly inhibited PGC-1α- and ERRα-induced activation of the PPARα promoter (Figure 4F) means that p300ΔC/H3 exerts inhibitory effects on both the expression and function of PGC-1α, thereby suppressing expression of multiple mitochondrial genes in p300ΔC/H3-TG mice.

Abnormal Mitochondrial Function in p300ΔC/H3-TG Hearts

To evaluate the function of mitochondria in p300ΔC/H3-TG hearts, we initially stained isolated ventricular myocytes with TMRE, a fluorescent dye whose accumulation in active mitochondria is dependent on the mitochondrial membrane potential. Examination of individual mitochondria revealed that TMRE fluorescence reflecting the mitochondrial membrane potential was disorganized and sparse, whereas mean TMRE signals from individual mitochondria were significantly weaker in ventricular myocytes isolated from p300ΔC/H3-TG mice than in those from WT mice (Figure 5A and 5B). We also used 2-photon laser microscopy to examine the mitochondrial membrane potential ex vivo in Langendorff-perfused p300ΔC/H3-TG hearts.[27] Again the fluorescent signals from the mitochondria in p300ΔC/H3-TG myocytes were significantly weaker than those from WT myocytes (Figure 5C and 5D), which confirmed the disruption of mitochondrial function in p300ΔC/H3-TG hearts. In addition, we subjected p300ΔC/H3-TG and WT hearts perfused with TMRE to global ischemia by clamping off the perfusion line and then monitored TMRE fluorescence in the ischemic hearts (Figure 5E). We observed a time-dependent loss of TMRE fluorescence, indicating depolarization of the mitochondrial membrane, in all of the ischemic hearts (Figure 5F). Notably, however, both the time course of the change in TMRE fluorescence (Figure 5F) and the average TMRE signals from individual cells (Figure 5G and 5H) in WT and p300ΔC/H3-TG hearts subjected to ischemia clearly showed that the depolarization was significantly greater in p300ΔC/H3-TG hearts than in WT hearts (Figure 5F, 5G and 5H). Moreover, the ATP content of p300ΔC/H3-TG hearts was significantly lower than in WT hearts (Figure 5I).

Increased Autophagic Myocardial Cell Death in p300ΔC/H3-TG

Mitochondrial dysfunction can lead to cell death through induction of apoptosis by release of cytochrome *c* and

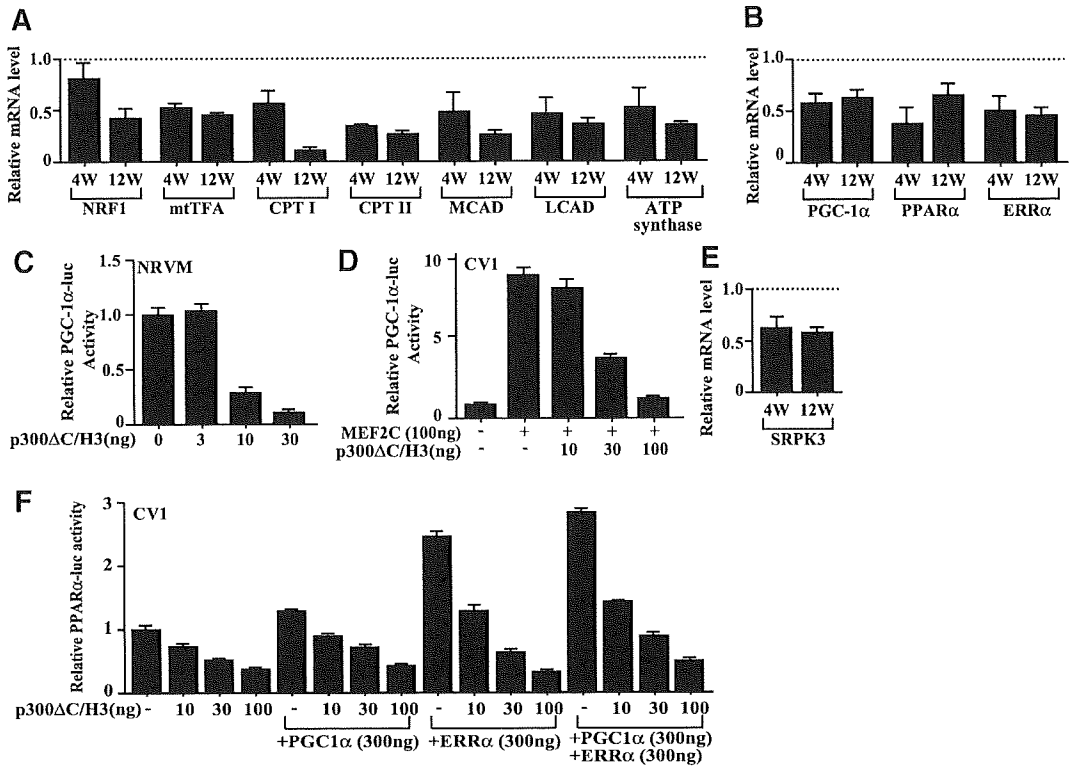

Figure 4. Reduced expression of mitochondrial genes in p300ΔC/H3-TG ventricles. A and B, Levels of mRNA expression of mitochondrial genes in p300ΔC/H3-TG normalized to the level in WT hearts were examined using real-time quantitative RT-PCR. The graphs show the relative levels of the indicated mRNAs normalized to the level of GAPDH mRNA in p300ΔC/H3-TG hearts and then further normalized to the levels in age-matched WT controls. $P<0.05$ between WT and p300ΔC/H3-TG hearts in all genes at both 4 and 12 weeks of age. CPT indicates carnitine palmitoyltransferase; LCAD, long-chain acyl-coenzyme A dehydrogenase; MCAD, medium-chain acyl-coenzyme A dehydrogenase. C and D, Luciferase activity of PCG-1α-luc in neonatal ventricular myocytes (NRVM, C) or CV1 cells (D) cotransfected with p300ΔC/H3 (C) or p300ΔC/H3+MEF2C (D). E, Levels of SRPK3 mRNA in p300ΔC/H3-TG hearts relative to those in WT hearts were examined using real-time quantitative RT-PCR. $P<0.05$ between WT and p300ΔC/H3-TG hearts. F, Luciferase activity of PPARα-luc in CV1 cells, cotransfected with p300ΔC/H3, PGC-1α and ERRα. In all of these experiments, luciferase activities in cells transfected with the reporter construct alone were assigned a value of 1.0. In all graphs, bars represent means±SEM.

subsequent activation of the caspase cascade, or through autophagic cell death mediated by cross-talk between the mitochondria and Golgi apparatus.[35] We then carried out Evans blue dye assays to compare the incidences of myocardial cell death in p300ΔC/H3-TG and WT hearts.[36] As shown in Figure 6A and 6B, intraperitoneally injected Evans blue labeled numerous cells in p300ΔC/H3-TG hearts, indicating the presence of ongoing cell death, but not in WT hearts. Electron microscopic examination of several degenerative myocytes in p300ΔC/H3-TG hearts revealed the presence of cytosolic vacuoles containing lipid droplets, myelin fibers, and degenerated mitochondria, typical features of autophagosomes (Figure 6C). Finally, Western blot analysis showed increased expression of LC3-II and cathepsin D, 2 markers of autophagic cell death, in p300ΔC/H3-TG hearts (Figure 6D). By contrast, agarose gel electrophoresis of genomic DNA provided no evidence of the DNA laddering characteristic of apoptosis (Figure 6E). In addition, there was no increase in the cleavage of caspase 3, a critical event in the activation of mitochondrial apoptotic pathways (Figure 6F).

Discussion

To evaluate the physiological function of p300 in postnatal hearts, we analyzed mice overexpressing a dominant negative p300 mutant (p300ΔC/H3) under the control of the α-MHC promoter. We found that LV function was disrupted in p300ΔC/H3-TG mice and that almost all died of heart failure by 20 weeks of age. p300ΔC/H3-TG hearts showed several mitochondrial abnormalities affecting both their structure and function. Expression of PGC-1α, a master regulator of mitochondrial gene expression,[15] and its target genes were markedly diminished in p300ΔC/H3-TG hearts. p300ΔC/H3 directly inhibited both the expression of PGC-1α and its transcriptional activity and also inhibited the transcriptional activity of ERRα, another regulator of mitochondrial gene expression. Consistent with these findings, mitochondrial membrane potential was severely depolarized in p300ΔC/H3-TG mice. Thus p300 appears to play an essential role in maintaining mitochondrial integrity in postnatal hearts, and its inhibition in adult hearts can lead to mitochondrial and LV dysfunction and death.

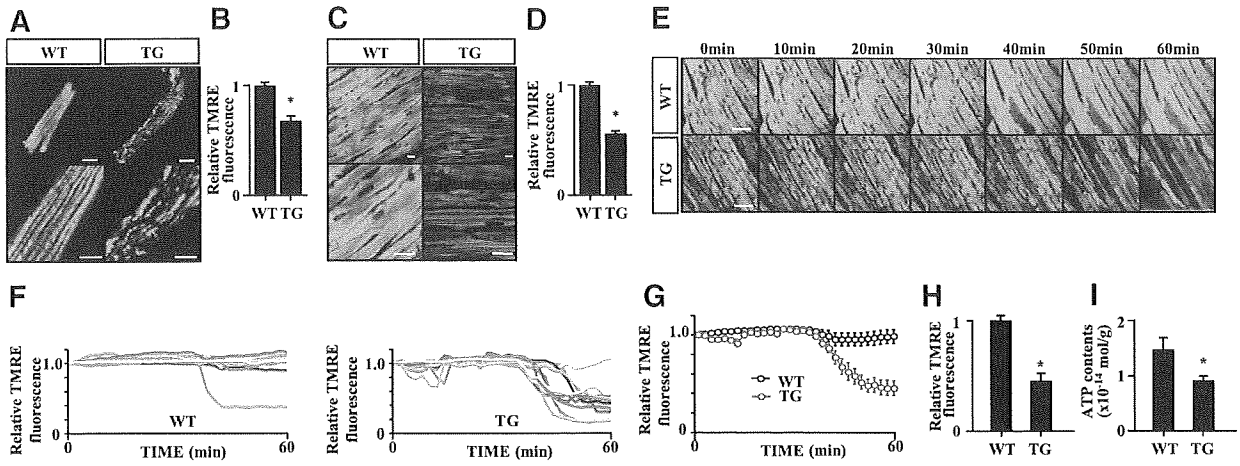

Figure 5. Reduced TMRE fluorescence in cardiomyocytes from p300ΔC/H3-TG hearts. A, Images of isolated TMRE-stained ventricular myocytes from WT and p300ΔC/H3-TG hearts. Scale bars=20 μm (top) or 10 μm (bottom). B, TMRE fluorescence of each mitochondrion in TMRE loaded isolated cardiac myocyte. The average of relative TMRE fluorescence of mitochondrion in WT cardiac myocytes was assigned a value of 1.0. C, Imaging of mitochondria in WT and p300ΔC/H3-TG hearts perfused with Tyrode's solution containing TMRE using the Langendorff method. Scale bar=20 μm. D, TMRE fluorescence of each mitochondrion of TMRE perfused in ex vivo mouse hearts. The average of relative TMRE fluorescence of mitochondrion in WT hearts was assigned a value of 1.0. E, Representative images showing progressive loss of mitochondrial membrane potential during ischemia. Images were acquired every 10 minutes. Images are from a single experiment representative of at least 3 independent experiments. Scale bar=50 μm. F, Time course of relative TMRE fluorescence intensities in several individual cells monitored at 2-minute intervals. TMRE fluorescence intensity at 0 minutes in each cell was assigned a value of 1.0. G, Average of relative TMRE fluorescence intensities in individual cells of WT and p300ΔC/H3-TG hearts monitored at 2-minute intervals. TMRE fluorescence intensity at 0 minutes in each cell was assigned a value of 1.0. H, TMRE fluorescence from individual cells in WT and p300ΔC/H3-TG hearts subjected to ischemia for 60 minutes. The relative TMRE fluorescence in WT hearts subjected to ischemia for 60 minutes was assigned a value of 1.0. I, ATP contents in WT and p300ΔC/H3-TG hearts. In all graphs, bars represent means±SEM.

It is known that PGC-1α, ERRα and PPARα act in concert to regulate mitochondrial biogenesis through the regulation of mitochondrial gene expression.[14,15,17] PGC-1α regulates the expression and transcriptional activity of ERRα,[37] whereas PGC-1α and ERRα act synergistically to activate the PPARα promoter.[13] Although p300 reportedly interacts with both PGC-1α and PPARα, its role in the transcriptional control of mitochondrial gene expression is not fully understood.[18–20] In the present study, we found that p300 is an indispensable component of the transcriptional pathways via which mitochondrial gene expression is regulated in adult ventricles. Indeed, transcription of ERRα, PPARα, and PGC-1α was significantly downregulated in p300ΔC/H3-TG hearts, which would in turn disrupt expression of an array of mitochondrial genes, leading to severe structural and functional abnormalities in mitochondria from p300ΔC/H3-TG mice.

p300 also serves as a cofactor for the cardiac-enriched transcription factors GATA4 and MEF2, which participate in the transcriptional regulation of fetal cardiac genes such as ANP and BNP.[7,38] Here, we confirmed that p300ΔC/H3 significantly inhibits GATA4- and MEF2-dependent promoter activity in cultured cells and showed that the activities of the ANP and BNP promoters were diminished by p300ΔC/H3 in cultured neonatal rat ventricular myocytes and noncardiomyocytes. Unexpectedly, however, expression of ANP and BNP mRNA was strongly upregulated in p300ΔC/H3-TG hearts (Figure 3A). Although it is clear that p300 coactivates GATA4 and MEF2C, our data suggest that p300 is dispensable for the pathological induction of ANP and BNP expression in the adult heart.

Mitochondria play a crucial role in the regulation of cell survival. Their dysfunction can lead to apoptosis, autophagy, and other modes of cell death via various pathways involving caspase activation, endoplasmic/sarcoplasmic reticulum–mitochondria connections and lysosome-mitochondria crosstalk.[35] In the present study, we found that the abnormal mitochondrial gene expression and function seen in p300ΔC/H3-TG hearts led to myocardial cell death that, at least in part, was caused by autophagy; we found no evidence of apoptotic cell death. Consistent with those results are the recent findings that mitochondrial apoptotic pathways are defective in cardiac myocytes.[39–41] For instance, the expression of apoptotic peptidase activating factor-1, an essential mediator of mitochondrial apoptotic death pathways, is suppressed in cardiac myocytes, making them resistant to mitochondria-mediated apoptosis.[41]

In summary, we found that, through the regulation of transcriptional pathways controlling mitochondrial gene expression, p300 is critically involved in the maintenance of mitochondrial integrity and cell survival in adult ventricles. These findings provide novel insight that could be useful in the development of new therapeutic strategies aimed at

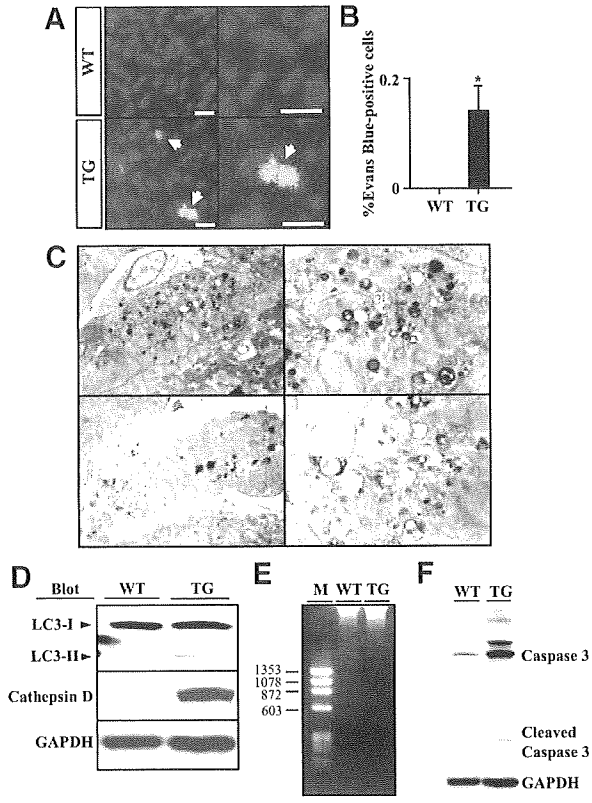

Figure 6. Analysis of cell death in p300ΔC/H3-TG hearts. A, Myocardia of a WT and a p300ΔC/H3-TG mouse intraperitoneally injected with Evans blue dye are shown. Red fluorescence indicates uptake of Evans blue (cell death). The nuclei appear blue. Scale bars=10 μm. B, Graphs show the numbers of Evans blue positive cells in WT and p300ΔC/H3-TG hearts. Bars represent means±SEM. C, Transmission electron micrographs of cardiac myocytes from a 12-weeks-old p300ΔC/H3-TG mouse showing the presence of autophagosomes. Left images show lower magnification; right images, higher magnification. D, Western blot analysis of LC-3 and cathepsin D in hearts from 12-week-old WT and p300ΔC/H3-TG mice. E, Ladder analysis of genomic DNA from 12-week-old WT and p300ΔC/H3-TG mice. F, Western blot analysis of full-length and cleaved caspase-3 in cardiac tissue from 12-week-old WT and p300ΔC/H3-TG mice.

preserving cardiac mitochondrial function through the enhancement of p300 activity.

Acknowledgments

We thank Y. Kubo for excellent secretarial work. We also thank N. Mizushima for providing the anti-LC3 antibody.

Sources of Funding

This research was supported by a Grant-in-Aid for Scientific Research from the Japan Society for the Promotion of Science (to K.K., M.H., and K.N.) and grants from the Japanese Ministry of Health, Labor and Welfare (to K.N.); the Japan Heart Foundation/Pfizer Pharmaceuticals Inc Grant on Cardiovascular Disease Research; the Japan Heart Foundation/Novartis Grant for Research Award on Molecular and Cellular Cardiology; the Mochida Memorial Foundation for Medical and Pharmaceutical Research; the Uehara Memorial Foundation; the Ichiro Kanehara Foundation; the Astellas Foundation for Research on Metabolic Disorders; the Mitsubishi Foundation; the Suzuken Memorial Foundation; the Takeda Medical Research Foundation; and the Kanae Foundation for the Promotion of Medical Science (to K.K.).

Disclosures

None.

References

1. Ogryzko VV, Schiltz RL, Russanova V, Howard BH, Nakatani Y. The transcriptional coactivators p300 and CBP are histone acetyltransferases. *Cell*. 1996;87:953–959.
2. Eckner R, Ewen ME, Newsome D, Gerdes M, DeCaprio JA, Lawrence JB, Livingston DM. Molecular cloning and functional analysis of the adenovirus E1A-associated 300-kD protein (p300) reveals a protein with properties of a transcriptional adaptor. *Genes Dev*. 1994;8:869–884.
3. Yao TP, Oh SP, Fuchs M, Zhou ND, Ch'ng LE, Newsome D, Bronson RT, Li E, Livingston DM, Eckner R. Gene dosage-dependent embryonic development and proliferation defects in mice lacking the transcriptional integrator p300. *Cell*. 1998;93:361–372.
4. Dai YS, Markham BE. p300 Functions as a coactivator of transcription factor GATA-4. *J Biol Chem*. 2001;276:37178–37185.
5. Slepak TI, Webster KA, Zang J, Prentice H, O'Dowd A, Hicks MN, Bishopric NH. Control of cardiac-specific transcription by p300 through myocyte enhancer factor-2D. *J Biol Chem*. 2001;276:7575–7585.
6. Kakita T, Hasegawa K, Morimoto T, Kaburagi S, Wada H, Sasayama S. p300 protein as a coactivator of GATA-5 in the transcription of cardiac-restricted atrial natriuretic factor gene. *J Biol Chem*. 1999;274:34096–34102.
7. Yanazume T, Hasegawa K, Morimoto T, Kawamura T, Wada H, Matsumori A, Kawase Y, Hirai M, Kita T. Cardiac p300 is involved in myocyte growth with decompensated herat failure. *Mol Cell Biol*. 2003;23:3593–3606.
8. Miyamoto S, Kawamura T, Morimoto T, Ono K, Wada H, Kawase Y, Matsumori A, Nishio R, Kita T, Hasegawa K. Histone acetyltransferase activity of p300 is required for the promotion of left ventricular remodeling after myocardial infarction in adult mice in vivo. *Circulation*. 2006;113:679–690.
9. Morimoto T, Sunagawa Y, Kawamura T, Takaya T, Wada H, Nagasawa A, Komeda M, Fujita M, Shimatsu A, Kita T, Hasegawa K. The dietary compound curcumin inhibits p300 histone acetyltransferase activity and prevents heart failure in rats. *J Clin Invest*. 2008;118:868–878.
10. Shikama N, Lutz W, Kretzschmar R, Sauter N, Roth JF, Marino S, Wittwer J, Scheidweiler A, Eckner R. Essential function of p300 acetyltransferase activity in heart, lung and small intestine formation. *EMBO J*. 2003;22:5175–5185.
11. Kawamura T, Hasegawa K, Morimoto T, Iwai-Kanai E, Miyamoto S, Kawase Y, Ono K, Wada H, Akao M, Kita T. Expression of p300 protects cardiac myocytes from apoptosis in vivo. *Biochem Biophys Res Commun*. 2004;315:733–738.
12. Lehman JJ, Barger PM, Kovacs A, Saffitz JE, Medeiros DM, Kelly DP. Peroxisome proliferator-activated receptor gamma coactivator-1 promotes cardiac mitochondrial biogenesis. *J Clin Invest*. 2000;106:847–856.
13. Huss JM, Torra IP, Staels B, Giguere V, Kelly DP. Estrogen-related receptor alpha directs peroxisome proliferator-activated receptor alpha signaling in the transcriptional control of energy metabolism in cardiac and skeletal muscle. *Mol Cell Biol*. 2004;24:9079–9091.
14. Gulick T, Cresci S, Caira T, Moore DD, Kelly DP. The peroxisome proliferator-activated receptor regulates mitochondrial fatty acid oxidative enzyme gene expression. *Proc Natl Acad Sci U S A*. 1994;91:11012–11016.
15. Finck BN, Kelly DP. Peroxisome proliferator-activated receptor gamma coactivator-1 (PGC-1) regulatory cascade in cardiac physiology and disease. *Circulation*. 2007;115:2540–2548.
16. Puigserver P, Wu Z, Park CW, Graves R, Wright M, Spiegelman BM. A cold-inducible coactivator of nuclear receptors linked to adaptive thermogenesis. *Cell*. 1998;92:829–839.
17. Schreiber SN, Emter R, Hock MB, Knutti D, Cardenas J, Podvinec M, Oakeley EJ, Kralli A. The estrogen-related receptor alpha (ERRalpha) functions in PPARgamma coactivator 1alpha (PGC-1alpha)-induced mitochondrial biogenesis. *Proc Natl Acad Sci U S A*. 2004;101:6472–6477.
18. Puigserver P, Adelmant G, Wu Z, Fan M, Xu J, O'Malley B, Spiegelman BM. Activation of PPARgamma coactivator-1 through transcription factor docking. *Science*. 1999;286:1368–1371.

19. Wallberg AE, Yamamura S, Malik S, Spiegelman B, Roeder RG. Coordination of p300-mediated chromatin remodeling and TRAP/mediator function through coactivator PGC-1a. *Mol Cell*. 2003;12:1137–1149.
20. Dowell P, Ishmael JE, Avram D, Peterson VJ, Nevrivy DJ, Leid M. p300 functions as a coactivator for the peroxisome proliferator-activated receptor alpha. *J Biol Chem*. 1997;272:33435–33443.
21. Kuwahara K, Saito Y, Ogawa E, Takahashi N, Nakagawa Y, Naruse Y, Harada M, Hamanaka I, Izumi T, Miyamoto Y, Kishimoto I, Kawakami R, Nakanishi M, Mori N, Nakao K. The neuron-restrictive silencer element-neuron-restrictive silencer factor system regulates basal and endothelin 1-inducible atrial natriuretic peptide gene expression in ventricular myocytes. *Mol Cell Biol*. 2001;21:2085–2097.
22. Ogawa E, Saito Y, Kuwahara K, Harada M, Miyamoto Y, Hamanaka I, Kajiyama N, Takahashi N, Izumi T, Kawakami R, Kishimoto I, Naruse Y, Mori N, Nakao K. Fibronectin signaling stimulates BNP gene transcription by inhibiting neuron-restrictive silencer element-dependent repression. *Cardiovasc Res*. 2002;53:451–459.
23. Nakagawa O, Ogawa Y, Itoh H, Suga S, Komatsu Y, Kishimoto I, Nishino K, Yoshimasa T, Nakao K. Rapid transcriptional activation and early mRNA turnover of brain natriuretic peptide in cardiocyte hypertrophy. Evidence for brain natriuretic peptide as an "emergency" cardiac hormone against ventricular overload. *J Clin Invest*. 1995;96:1280–1287.
24. Kuwahara K, Saito Y, Takano M, Arai Y, Yasuno S, Nakagawa Y, Takahashi N, Adachi Y, Takemura G, Horie M, Miyamoto Y, Morisaki T, Kuratomi S, Noma A, Fujiwara H, Yoshimasa Y, Kinoshita H, Kawakami R, Kishimoto I, Nakanishi M, Usami S, Saito Y, Harada M, Nakao K. NRSF regulates the fetal cardiac gene program and maintains normal cardiac structure and function. *EMBO J*. 2003;22:6310–6321.
25. Kabeya Y, Mizushima N, Ueno T, Yamamoto A, Kirisako T, Noda T, Kominami E, Ohsumi Y, Yoshimori T. LC3, a mammalian homologue of yeast Apg8p, is localized in autophagosome membranes after processing. *EMBO J*. 2000;19:5720–5728.
26. Kuma A, Hatano M, Matsui M, Yamamoto A, Nakaya H, Yoshimori T, Ohsumi Y, Tokuhisa T, Mizushima N. The role of autophagy during the early neonatal starvation period. *Nature*. 2004;432:1032–1036.
27. Matsumoto-Ida M, Akao M, Takeda T, Kato M, Kita T. Real-time 2-photon imaging of mitochondrial function in perfused rat hearts subjected to ischemia/reperfusion. *Circulation*. 2006;114:1497–1503.
28. De Luca A, Severino A, De Paolis P, Cottone G, De Luca L, De Falco M, Porcellini A, Volpe M, Condorelli G. p300/cAMP-response-element-binding-protein ('CREB')-binding protein (CBP) modulates co-operation between myocyte enhancer factor 2A (MEF2A) and thyroid hormone receptor-retinoid X receptor. *Biochem J*. 2003;369:477–484.
29. Avantaggiati ML, Ogryzko V, Gardner K, Giordano A, Levine AS, Kelly K. Recruitment of p300/CBP in p53-dependent signal pathways. *Cell*. 1997;89:1175–1184.
30. Yang XJ, Ogryzko VV, Nishikawa J, Howard BH, Nakatani Y. A p300/CBP-associated factor that competes with the adenoviral oncoprotein E1A. *Nature*. 1996;382:319–324.
31. Saito Y, Nakao K, Arai H, Nishimura K, Okumura K, Obata K, Takemura G, Fujiwara H, Sugawara A, Yamada T. Augmented expression of atrial natriuretic polypeptide gene in ventricle of human failing heart. *J Clin Invest*. 1989;83:298–305.
32. Mukoyama M, Nakao K, Hosoda K, Suga S, Saito Y, Ogawa Y, Shirakami G, Jougasaki M, Obata K, Yasue H. Brain natriuretic peptide as a novel cardiac hormone in humans. Evidence for an exquisite dual natriuretic peptide system, atrial natriuretic peptide and brain natriuretic peptide. *J Clin Invest*. 1991;87:1402–1412.
33. Czubryt MP, McAnally J, Fishman GI, Olson EN. Regulation of peroxisome proliferator-activated receptor gamma coactivator 1 alpha (PGC-1 alpha) and mitochondrial function by MEF2 and HDAC5. *Proc Natl Acad Sci U S A*. 2003;100:1711–1716.
34. Wei JQ, Shehadeh LA, Mitrani JM, Pessanha M, Slepak TI, Webster KA, Bishopric NH. Quantitative control of adaptive cardiac hypertrophy by acetyltransferase p300. *Circulation*. 2008;118:934–946.
35. Kim R, Emi M, Tanabe K. Role of mitochondria as the gardens of cell death. *Cancer Chemother Pharmacol*. 2006;57:545–553.
36. Miyata S, Takemura G, Kawase Y, Li Y, Okada H, Maruyama R, Ushikoshi H, Esaki M, Kanamori H, Li L, Misao Y, Tezuka A, Toyo-Oka T, Minatoguchi S, Fujiwara T, Fujiwara H. Autophagic cardiomyocyte death in cardiomyopathic hamsters and its prevention by granulocyte colony-stimulating factor. *Am J Pathol*. 2006;168:386–397.
37. Schreiber SN, Knutti D, Brogli K, Uhlmann T, Kralli A. The transcriptional coactivator PGC-1 regulates the expression and activity of the orphan nuclear receptor estrogen-related receptor alpha (ERRalpha). *J Biol Chem*. 2003;278:9013–9018.
38. Gusterson R, Brar B, Faulkes D, Giordano A, Chrivia J, Latchman D. The transcriptional co-activators CBP and p300 are activated via phenylephrine through the p42/p44 MAPK cascade. *J Biol Chem*. 2002;277:2517–2524.
39. Kanoh M, Takemura G, Misao J, Hayakawa Y, Aoyama T, Nishigaki K, Noda T, Fujiwara T, Fukuda K, Minatoguchi S, Fujiwara H. Significance of myocytes with positive DNA in situ nick end-labeling (TUNEL) in hearts with dilated cardiomyopathy: not apoptosis but DNA repair. *Circulation*. 1999;99:2757–2764.
40. Takemura G, Fujiwara H. Morphological aspects of apoptosis in heart diseases. *J Cell Mol Med*. 2006;10:56–75.
41. Bahi N, Zhang J, Llovera M, Ballester M, Comella JX, Sanchis D. Switch from caspase-dependent to caspase-independent death during heart development: essential role of endonuclease G in ischemia-induced DNA processing of differentiated cardiomyocytes. *J Biol Chem*. 2006;281:22943–22952.

T-Type Ca^{2+} Channel Blockade Prevents Sudden Death in Mice With Heart Failure

Hideyuki Kinoshita, MD; Koichiro Kuwahara, MD, PhD; Makoto Takano, MD, PhD; Yuji Arai, MD, PhD; Yoshihiro Kuwabara, MD; Shinji Yasuno, MD; Yasuaki Nakagawa, MD, PhD; Michio Nakanishi, MD, PhD; Masaki Harada, MD, PhD; Masataka Fujiwara, MD; Masao Murakami, PhD; Kenji Ueshima, MD, PhD; Kazuwa Nakao, MD, PhD

Background—Pharmacological interventions for prevention of sudden arrhythmic death in patients with chronic heart failure remain limited. Accumulating evidence suggests increased ventricular expression of T-type Ca^{2+} channels contributes to the progression of heart failure. The ability of T-type Ca^{2+} channel blockade to prevent lethal arrhythmias associated with heart failure has never been tested, however.

Methods and Results—We compared the effects of efonidipine and mibefradil, dual T- and L-type Ca^{2+} channel blockers, with those of nitrendipine, a selective L-type Ca^{2+} channel blocker, on survival and arrhythmogenicity in a cardiac-specific, dominant-negative form of neuron-restrictive silencer factor transgenic mice (dnNRSF-Tg), which is a useful mouse model of dilated cardiomyopathy leading to sudden death. Efonidipine, but not nitrendipine, substantially improved survival among dnNRSF-Tg mice. Arrhythmogenicity was dramatically reduced in dnNRSF-Tg mice treated with efonidipine or mibefradil. Efonidipine acted by reversing depolarization of the resting membrane potential otherwise seen in ventricular myocytes from dnNRSF-Tg mice and by correcting cardiac autonomic nervous system imbalance. Moreover, the *R*(−)-isomer of efonidipine, a recently identified, highly selective T-type Ca^{2+} channel blocker, similarly improved survival among dnNRSF-Tg mice. Efonidipine also reduced the incidence of sudden death and arrhythmogenicity in mice with acute myocardial infarction.

Conclusions—T-type Ca^{2+} channel blockade reduced arrhythmias in a mouse model of dilated cardiomyopathy by repolarizing the resting membrane potential and improving cardiac autonomic nervous system imbalance. T-type Ca^{2+} channel blockade also prevented sudden death in mice with myocardial infarction. Our findings suggest T-type Ca^{2+} channel blockade is a potentially useful approach to preventing sudden death in patients with heart failure. (***Circulation.* 2009;120:743-752.**)

Key Words: ion channels ■ nervous system, autonomic ■ heart failure ■ calcium ■ arrhythmia

As many as 50% of deaths among heart failure patients are sudden and unexpected, presumably the result of lethal arrhythmias.[1] Despite recent progress in nonpharmacological therapy, pharmacological interventions for the treatment and prevention of lethal arrhythmias associated with chronic heart failure remain limited. A prerequisite for the development of new pharmacological approaches is to identify potential targets based on knowledge of the molecular basis of arrhythmogenesis in failing hearts.

Clinical Perspective on p 752

Compelling evidence implicates T-type Ca^{2+} channels in the progression of heart failure.[2,3] During development, T-type Ca^{2+} channels are abundantly expressed in the embryonic ventricle, but their expression is suppressed in the adult ventricle, so that it is restricted to the conduction system.[4,5] However, T-type Ca^{2+} channels are reexpressed in hypertrophied and failing ventricles,[4,6–9] and the resultant T-type Ca^{2+} currents ($I_{Ca,T}$) are thought to be involved in the pathological process that leads to systolic dysfunction and arrhythmogenesis.[2,9] Indeed, several studies have shown that mibefradil, which blocks both T- and L-type Ca^{2+} channels, mitigates the functional deterioration of the ventricle in some animal models of heart failure.[10–12] More recently, it was shown that the genetic deletion of *CACNA1H*, which encodes the α1H T-type Ca^{2+} channel, resulted in resistance to pathological

Received February 12, 2009; accepted June 23, 2009.

From the Department of Medicine and Clinical Science (H.K., K.K., Y.K., S.Y., Y.N., M.N., M.H., M.F., M.M., K.N.), Kyoto University Graduated School of Medicine, Kyoto, Japan; Department of Biophysics (M.T.), Jichi Medical School, Shimotsuke, Japan; Department of Bioscience (Y.A.), National Cardiovascular Center Research Institute, Suita, Japan; and EBM Research Center (K.U.), Kyoto University Graduate School of Medicine, Kyoto, Japan.

The online-only Data Supplement is available with this article at http://circ.ahajournals.org/cgi/content/full/CIRCULATIONAHA.109.857011/DC1.

Correspondence to Koichiro Kuwahara, MD, PhD, Department of Medicine and Clinical Science, Kyoto University Graduated School of Medicine, 54 Shogoin Kawaracho, Sakyo-ku, Kyoto, Japan 606-8507. E-mail kuwa@kuhp.kyoto-u.ac.jp

Circulation **is available at http://circ.ahajournals.org** **DOI: 10.1161/CIRCULATIONAHA.109.857011**

cardiac hypertrophy.[9] The ability of T-type Ca^{2+} channel blockade to prevent malignant arrhythmia and sudden death associated with heart failure remains unevaluated, however.

We recently reported that a transcriptional repressor, neuron-restrictive silencer factor (NRSF, also called REST), is an important regulator of the fetal cardiac gene program.[13] Transgenic mice that selectively express a dominant-negative form of NRSF (dnNRSF) in their hearts (dnNRSF-Tg) showed progressive cardiomyopathy and sudden arrhythmic death beginning at ≈8 weeks of age.[14] The dnNRSF-Tg hearts showed increased expression of fetal-type ion channel genes, including *CACNA1H*, which encodes the T-type Ca^{2+} channel α-subunit. Moreover, $I_{Ca,T}$ amplitude was correspondingly increased in ventricular myocytes from dnNRSF-Tg hearts, which suggests that $I_{Ca,T}$ in some way contributes to the susceptibility of dnNRSF-Tg hearts to arrhythmias.[14]

To clarify the contribution made by T-type Ca^{2+} channels to the development of malignant arrhythmias and to assess the ability of T-type Ca^{2+} channel blockade to prevent sudden death associated with heart failure, we compared the effects of efonidipine and mibefradil, dual T- and L-type Ca^{2+} channel blockers,[15,16] with those of nitrendipine, a more L-type–selective Ca^{2+} channel blocker, on survival and arrhythmogenicity in dnNRSF-Tg mice and mice with myocardial infarction. We also tested the effects of the *R*(−)-isomer of efonidipine [*R*(−)-efonidipine], a recently identified, highly selective T-type Ca^{2+} channel blocker, on dnNRSF-Tg mice.[17,18] Our findings demonstrate that T-type Ca^{2+} channel blockade may represent a new and effective means of preventing sudden cardiac death in patients with heart failure.

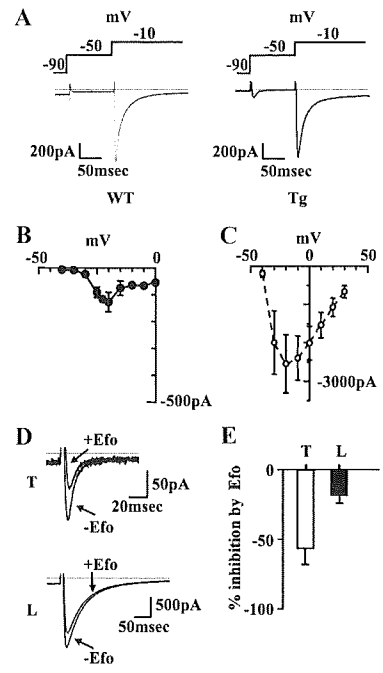

Figure 1. $I_{Ca,T}$ in ventricular myocytes from dnNRSF-Tg mice. A, Ca^{2+} currents recorded in WT (left) and dnNRSF-Tg (Tg; right) mouse. The double-pulse protocol is shown at the top. Na^+ currents were suppressed by use of Na^+-free bathing solution. $I_{Ca,T}$ were elicited at −50 mV only in dnNRSF mice. B, Current-voltage relationship for $I_{Ca,T}$ in cardiomyocytes from dnNRSF mice (n=5). At membrane potentials more positive than −40 mV, peak amplitudes of inward currents elicited from a conditioning potential of −90 or −50 mV were subtracted. C, Current-voltage relationship for $I_{Ca,L}$ in cardiomyocytes from dnNRSF mice. The conditioning potential was −50 mV (n=5). D, Effect of efonidipine (Efo) 10 μmol/L on $I_{Ca,T}$ (T) and $I_{Ca,L}$ (L). In the top panel, $I_{Ca,T}$ was activated by depolarization to −45 mV from a holding potential of −80 mV. Bottom panel, $I_{Ca,L}$ recorded from a myocyte from a WT mouse. $I_{Ca,L}$ was activated by depolarization to −10 mV from a holding potential of −80 mV. E, Summary of the inhibitory effects of efonidipine (Efo; 10 μmol/L) on $I_{Ca,T}$ (T) and $I_{Ca,L}$ (L) in ventricular myocytes. Efonidipine reduced the amplitudes of $I_{Ca,T}$ by 57±12% (n=4) while reducing the amplitudes of $I_{Ca,L}$ by 21±4% (n=5).

Methods

Animal Experiments

Animal care and all experimental protocols were conducted in accordance with the institutional guidelines of the Kyoto University Graduate School of Medicine. Beginning at 8 weeks of age, dnNRSF-Tg mice were left untreated (control) or were treated for 7 weeks with efonidipine (40 mg · kg^{-1} · d^{-1} PO) or nitrendipine (20 mg · kg^{-1} · d^{-1} PO). In another experiment, 10- or 11-week-old dnNRSF-Tg mice were left untreated (control) or treated for 7 days with mibefradil (15 mg · kg^{-1} · d^{-1}), efonidipine (200 mg · kg^{-1} · d^{-1}), or nitrendipine (60 mg · kg^{-1} · d^{-1}). The doses of mibefradil, efonidipine, and nitrendipine were chosen on the basis of earlier reports and our preliminary studies.[19–22]

In the experiment with *R*(−)-efonidipine, dnNRSF-Tg mice were left untreated (control) or were treated for 20 weeks with the *R*(−)-isomer efonidipine (200 mg · kg^{-1} · d^{-1} PO). Acute myocardial infarction was induced in female C57BL/6 mice (age 8 to 12 weeks; weight 19 to 24 g) by ligation of the left coronary artery as described previously.[23] Beginning 1 day after the operation, mice were left untreated (control) or were treated for 30 days with efonidipine hydrochloride (200 mg · kg^{-1} · d^{-1}) or nitrendipine (60 mg · kg^{-1} · d^{-1}).

Efonidipine and *R*(−)-isomer efonidipine were supplied by Nissan Chemical Industries, Ltd (Tokyo, Japan). Nitrendipine was purchased from Wako Pure Chemical Industries, Ltd (Osaka, Japan).

Patch-Clamp Studies

Myocytes were dispersed by a method described previously.[24] To record T- and L-type Ca^{2+} currents, electrodes were filled with Cs^+-rich solution that contained (in mmol/L): 100 CsCl, 50 NMDG, 10 TEA, 5 MgATP, 5 HEPES, and 10 EGTA (pH 7.2 with CsOH). After establishment of the ruptured whole-cell patch configuration in normal Tyrode solution, the bathing solution was switched to Na^+-free solution. A stock solution of efonidipine 10 mmol/L in DMSO was diluted to the desired concentration with Na^+-free bathing solution (final concentration 10 μmol/L).

Intracardiac Electrophysiology

A 1.7F octapolar catheter (CIBer mouse EP, NuMe, Hopkinton, NY) inserted via the jugular vein was used to perform a standard electrophysiological study protocol as described previously.[14,25]

Statistical Analysis

Data are presented as mean±SEM. Survival was analyzed by the Kaplan-Meier method with the log-rank test. ANOVA with post hoc Student-Newman-Keuls tests was used for comparisons among groups. Values of $P<0.05$ were considered significant. Repeated-measures analyses with linear mixed-effects models were performed with data comprising repeated observations made over time. Data obtained from the 2-way factorial design were analyzed with the 2-way ANOVA.